



## REVIEW ARTICLE

# CO<sub>2</sub> utilization as gas antisolvent for the pharmaceutical micro and nanoparticle production: A review



Nadia Esfandiari <sup>a,\*</sup>, Seyed Ali Sajadian <sup>b,c</sup>

<sup>a</sup> Department of Chemical Engineering, Marvdasht Branch, Islamic Azad University, Marvdasht, Iran

<sup>b</sup> Department of Chemical Engineering, Faculty of Engineering, University of Kashan, Postal Code: 87317-53153, Kashan, Iran

<sup>c</sup> South Zagros Oil and Gas Production, National Iranian Oil Company, Postal Code: 7135717991, Shiraz, Iran

Received 28 May 2022; accepted 30 July 2022

Available online 3 August 2022

## KEYWORDS

Gas antisolvent (GAS);  
Particle size;  
Experimental;  
Modeling;  
Nanoparticle

**Abstract** A reduction in particle size improves the solubility and bioavailability of pharmaceuticals. The traditional methods utilized in this regard are associated with problems so the use of supercritical fluid has been highlighted in recent decades. To prepare nanoparticles by employing the gas antisolvent (GAS) technique, a specific amount of solution (solute dissolved in organic solvent) was loaded into a cell in the oven. The supercritical carbon dioxide was injected and dissolved into the organic solvent. Therefore, volume expansion occurred and the solute was precipitated with a new particle size distribution on the filter at the end of the cell. This technique exhibits advantages such as particle size control, solvent-free product, and low-temperature process. Many experimental and modeling research has been conducted to synthesize nano- and microparticles based on the GAS process. The present study seeks to review the effective factors and literature on the GAS technique. All parameters affecting the GAS process including pressure, temperature, antisolvent addition rate, initial soluble concentration, and solvent were investigated. Volume expansion, thermodynamic modeling, and kinetic modeling of the GAS process were reviewed. A comparison was conducted between the advantages and disadvantages of this method with other methods of producing nanoparticles with supercritical fluid.

© 2022 The Authors. Published by Elsevier B.V. on behalf of King Saud University. This is an open access article under the CC BY-NC-ND license (<http://creativecommons.org/licenses/by-nc-nd/4.0/>).

## 1. Introduction

Most drugs have low bioavailability, a decrease in the particle size of which to nano and micro scale can enhance bioavailability and decline their consumption. The traditional methods for particle size reduction are accompanied by problems such as the change in the nature of drug particles because of heating and high mechanical tension, as well as the presence of solvent in the final product and lack of particle size control. Recently, much attention has been paid to the production of drug

\* Corresponding author.

E-mail address: [esfandiari\\_n@miau.ac.ir](mailto:esfandiari_n@miau.ac.ir) (N. Esfandiari).

Peer review under responsibility of King Saud University.



Production and hosting by Elsevier

### Nomenclature

$a_v(\text{m}^2/\text{m}^3)$	specific surface area of particles	P (Pa)	pressure
$b(\text{m}^3/\text{mol})$	parameter in the PR-EOS	$Q_A(\text{mol/s})$	molar flow rate of antisolvent
$B(\#/\text{m}^3 \text{ s})$	nucleation rate	R (J/mol K)	universal gas constant, $R = 8.314$
$B'(\#/\text{m}^3 \text{ s})$	primary nucleation	S	supersaturation
$B''(\#/\text{m}^3 \text{ s})$	secondary nucleation	t (s)	time
cv	coefficient of variation	T (K)	temperature
$c_p(\text{mol}/\text{m}^3)$	molar concentration of i in the liquid phase	$v_\alpha(\text{m}^3/\text{mol})$	molar volume of the $\alpha$ phase
D (m/s)	diffusion coefficient of the solute in the liquid phase	$x_i$	mole fraction of component i in liquid phase
$d_M(\text{m})$	molecular diameter	$y_i$	mole fraction of component i in vapor phase
F	objective function	z	compressibility factor
$f_p^L(\text{Pa})$	pure subcooled liquid fugacity of solute	<i>Greek letters</i>	
$f_p^S(\text{Pa})$	pure solid fugacity of solute	$\Delta$	property change
g	growth rate order with respect to supersaturation	$\varphi$	fugacity coefficient
G (m/s)	growth rate	$\alpha$	correction factor of attractive parameter
H (J/mol)	heat of fusion	$\gamma(\text{J}/\text{m}^2)$	interfacial tension
k (J/K)	Boltzmann's constant, $k = 1.38 \times 10^{-23}$	$\eta(\text{Pa} \cdot \text{s})$	dynamic viscosity of the liquid phase
$k_a$	surface shape factor	$\alpha''$	secondary nucleation rate coefficient
$k_g(\text{m/s})$	growth rate coefficient	<i>Superscripts and subscripts</i>	
$k_v$	volume shape factor	0	reference condition
$\underline{L}$ (m)	particle characteristic	i	species i
$\bar{L}(\text{m})$	mean distribution	tp	triple point
$m_i(\text{m}^i/\text{m}^3)$	ith moment of population density function	L	liquid
n ( $\#/\text{m}^4$ )	population density function	V	vapor
$N_A(1/\text{mol})$	Avogadro's number, $N_A = 6.022 \times 10^{23}$	S	solid
$N_\alpha(\text{mol})$	molar hold-up in the $\alpha$ phase		

nano- and microparticles by using the supercritical fluid technique. This technique can be applied to control product particle size and proper particle size distribution. The lack of solvent in the final product can be addressed as another benefit of using the method (Esfandiari 2015). An increase in the temperature and pressure in a pure substance decreases the compression of the liquid phase compression and enhances that of the gas phase. After reaching the temperature and pressure above the critical values, liquid and gas phases cannot be distinguished due to the formation of supercritical fluid with unique properties. Fig. 1 displays the supercritical fluid range. Supercritical fluids have special properties. The viscosity, density,

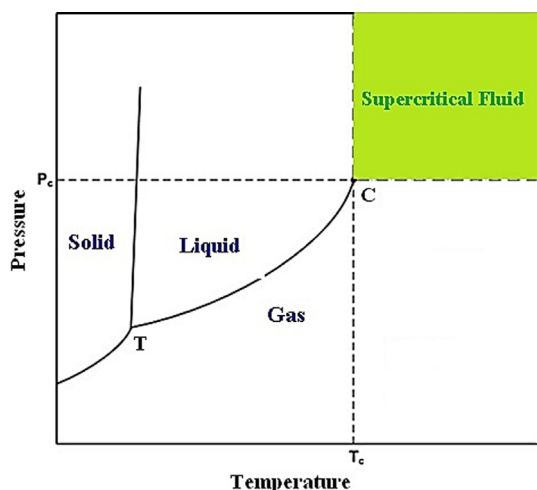


Fig. 1 Schematic phase diagram pure substance.

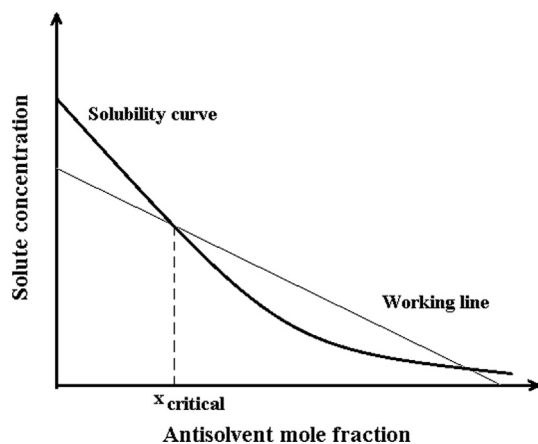
and diffusivity of supercritical fluids are between the liquid and gas. Table 1 summarizes the kinds of supercritical fluids, as well as their temperature, pressure, and density, by representing the low critical temperature and moderate critical pressure of carbon dioxide. In addition, carbon dioxide is inexpensive, non-toxic, and non-flammable. Therefore, this supercritical fluid has been highly highlighted and used in recent decades (Esfandiari 2015, Knez et al., 2019, Li and Xu 2019). Further, supercritical carbon dioxide is a conventional fluid in particle size reduction methods. In the case of utilizing supercritical carbon dioxide, its less critical temperature and moderate critical pressure do not lead to any change in the nature of the drug (Najafi 2021). The methods of drug nanoparticle preparation through using the supercritical fluid are classified according to the role of the fluid. Thus, the rapid expansion of the supercritical solution (RESS) process is employed when supercritical fluid acts as a solvent (Sodeifian et al., 2019, Han et al., 2021, Kumar et al., 2021, Sakabe and Uchida 2022, Türk 2022), while supercritical antisolvent (SAS) (Abuzar et al., 2018, Franco and De Marco 2021, Yan et al., 2021), gas antisolvent (GAS) (Amani 2021, Najafi 2021, Najafi 2021, Sodeifian et al., 2022), solution-enhanced dispersion by supercritical fluid (SEDS) (Kankala et al., 2018, Jia et al., 2019, Lee et al., 2019, Sachett et al., 2022, Xiao et al., 2022), and aerosol solvent extraction system (ASES) techniques (Lee et al., 2008, Yan et al., 2019, Kumar 2021) are utilized if the supercritical fluid plays the role of an antisolvent. The particles from the gas saturated solution (PGSS) process are used when supercritical fluid is solute (López-Iglesias et al., 2020, López-Iglesias et al., 2020, Tokunaga et al., 2021).

In the SAS process, the solute is dissolved in the organic solvent. This solution is injected through the nozzle in the cell that is filled with supercritical carbon dioxide. The supercritical carbon dioxide is diffused into the droplets of solution and solute precipitated. To prepare nanoparticles by employing the GAS technique, the solute is first dissolved in a solvent, a specific amount of solution is loaded into a cell.

**Table 1** Critical Properties of some compounds (Li and Xu 2019).

Substance	Critical temperature (°C)	Critical pressure (MPa)	Critical density (g/mL)
Water	374.15	22.05	0.322
Carbon dioxide	31.02	7.38	0.448
Ethane	32.19	4.87	0.203
Methane	-82.6	4.59	0.200
Ethylene	9.2	5.04	0.218
Propane	96.7	4.24	0.217
Nitrous oxide	36	7.28	0.450
Propylene	91.85	4.62	0.232
Xenon	16.55	5.87	0.118
Ammonia	132.45	11.28	0.325
Benzene	288.95	4.89	0.302
Toluene	318.55	4.11	0.292
Methanol	239.45	8.09	0.272
Ethanol	240.75	6.14	0.276
Acetone	234.95	4.7	0.278

This cell is placed in an oven for controlling temperature, to which supercritical carbon dioxide is injected. Carbon dioxide dissolves into the organic solvent. So volume expansion occurs. Then, the solute is precipitated with a new particle size distribution on the filter at the end of the cell. When carbon dioxide is dissolved in the solvent, the solubility of the solvent is reduced and when the amount of carbon dioxide reaches a critical amount, the reduction of solvent power occurs. Reduction in solvent power causes solute transfer from the liquid phase to the solid phase in the form of precipitated particles (Fig. 2). In the ASES method, the cell is filled with supercritical carbon dioxide, then the solution (solute + solvent) and supercritical carbon dioxide are sprayed into the cell by an atomization nozzle. In the SEDS, the solution and supercritical carbon dioxide are injected from a nozzle with the coaxial passage. The solubility of pharmaceuticals should be estimated in supercritical carbon dioxide to select a suitable method. Supercritical carbon dioxide is used as a solvent if the drug has a good dissolution capability in supercritical carbon dioxide. Otherwise, supercritical carbon dioxide is used as an antisolvent in the process. For this reason, the solubility of many pharmaceuticals in supercritical carbon dioxide has been measured experimentally (Esfandiari and Sajadian 2022, Sajadian et al., 2022, Sodeifian et al., 2022). On the

**Fig. 2** Solubility diagram in the GAS process (Ulker and Erkey 2017).

other hand, laboratory measurement of drug solubility in supercritical carbon dioxide requires a lot of cost and time. Therefore, solubility modeling is another way to access this information. Modeling of pharmaceuticals solubility was done by empirical and semi-empirical models and models based on the equation of state such as Peng-Robinson, Predictive Soave-Redlich-Kwong (Hazaveie et al., 2020, Sodeifian et al., 2020, Wang and Hsieh 2022). Reverchon and Adami investigated the preparation of nanoparticles via supercritical fluids (Reverchon and Adami 2006). The various methods were reviewed for producing nanoparticles of drugs by using supercritical fluid (Badens et al., 2018, Banchemo 2021, Kankala et al., 2021, Liu et al., 2021). The selection of supercritical methods for pharmaceutical micronization depends on the solubility of pharmaceuticals in supercritical carbon dioxide and solubility in the organic solvent (Franco and De Marco 2021). Campardelli et al. studied supercritical fluid application in nano drug production (Campardelli et al., 2015), while Nuchuchua et al. assessed nanoparticle release characteristics by applying supercritical carbon dioxide methods (Nuchuchua et al., 2017). Additionally, Smirnova and Gurikov collected laboratory data related to the placement of drugs in porous media (Smirnova and Gurikov 2017). Some researchers evaluated the technologies for liposome preparation like the use of supercritical fluid (Leitgeb et al., 2020). Microencapsulation and nanoencapsulation using supercritical fluid Methods are investigated for drug delivery (Padrela et al., 2018, Soh and Lee 2019). Micronization of food ingredients via supercritical carbon dioxide was interesting in recent years (Temelli 2018). The GAS process is obtained as the most potent method for the micronization of pharmaceuticals. The GAS is significant compared to the old methods of micronization due to the low to a moderate temperature of the process. These conditions are suitable for pharmaceuticals that are temperature sensitive. Product size distribution is narrower than the RESS method. Compared to PGSS and conventional micronization methods, particle size and particle size distribution can be controlled well with operating conditions (Padrela et al., 2018). The residual solvent in a final product with this method is lower than the standard limit by the United States Pharmacopoeia. The standard limit for benzene, carbon tetrachloride, acetonitrile, chloroform, and formamide were 2, 2, 410, 60, and 220 ppm, respectively (Foster et al., 2003). Another important point of this process is that the particle size and particle size distribution are controlled by parameters such as pressure, temperature, antisolvent addition rate, and initial solute concentration. The drawbacks of GAS are batch mode and small production capacity.

In this study, first, the reason for reducing particle size was suggested to increase solubility and biological absorption. Supercritical fluid types and characteristics and reasons for common use of supercritical carbon dioxide were investigated. The introduction section briefly presents articles that have been used for micronization with different methods of producing nanoparticles with supercritical fluid. Then, all parameters affecting the GAS process including pressure, temperature, antisolvent addition rate, initial soluble concentration, and solvent were investigated. Articles that produced nano and microparticles by the GAS method were investigated and the effect of each parameter was discussed. Table 2 was prepared and previous research was collected along with the value of parameters affecting particle size. Then thermodynamic modeling was investigated. Before GAS experiments, it is necessary to model thermodynamics to determine the temperature and pressure range that can precipitate particles. Various researches were reviewed. Then, in Table 8, the pressure and temperature ranges obtained from thermodynamic modeling for the ternary system (antisolvent-solvent-solute) with the equation of state and mixing rules were presented. Kinetic modeling of the GAS process was investigated to determine the nucleation and growth that affect particle size and particle size distribution. The results of kinetic modeling of different systems with the parameters value of modeling in Table 9 have been collected. Finally, the production of nanocomposites and co-crystal was investigated by the GAS method. Table 10 was prepared to compare the advantages and disadvantages of nanoparticle production methods with supercritical fluid.

**Table 2** Review of pharmaceutical micronization via a GAS process.

Pharmaceutical compound	Solvent	Antisolvent Addition Rate	Initial solute concentration	Temperature (°C)	Pressure (MPa)	Mean particle size	Objective of micronizing	Ref
Ampicillin	DMSO	1.2–2.4 mL/min	20–100 mg/mL	34–46	9–15	220–430 µm	Particle size reduction	(Esfandiari 2015)
Aspirin	Methanol, Acetone	8–40 bar/min	0.2, 0.27 g/g solution	37, 42	–	48–124 µm	Particle size reduction, effect of solvent on crystallinity	(Jafari et al., 2015)
Beclomethasone-1721-dipeopionate	Acetone	1–100 mL/min	5–100 %	25–52.5	68	1.8–43.9 µm	Particle size control, BECD powder for pulmonary inhalation therapy	(Bakbakhi et al., 2006)
Capecitabine	DMSO	–	15, 45, 75 mg/mL	35, 45, 55	12, 14, 16	243.3–1090.9 nm	Particle size reduction, dissolution rate increased	(Amani 2021)
Carbamazepine	Methanol,	1.52 g/s	70 mg/mL	40	9	–	Comparison between GAS and solvent evaporation	(Padrela et al., 2017)
Carbamazepine-Nicotinamide	Ethanol	90–95 mL/min	–	40	11	–	Cocrystallization, changed morphology from crystalline to amorphous.	(Shikhar et al., 2011)
β-carotene	Dichloromethane, Ethyl acetate	3, 70 g/min	1–2.4 g/L	25–40	5.8–7.8	0.5–5 µm	Particle size reduction	(Cocero and Ferrero 2002)
Cholesterol	Acetone	1–2.5 mL/min	3.5 wt%	35–45	0.1–7.5	–	Particle size reduction and solubility determined	(Liu et al., 2002)
Cimetidine	Methanol, Dichloromethane	–	–	40, 50, 70	15, 20, 25	3.1–26.7 µm	Particle size reduction, narrow particle size distribution	(Martausová 2016)
Copper Indomethacin	DMSO, DMF, NMP	2–4 mL/min	5–200 mg/g	25–40	6.6–14.5	< 100 µm	Cocrystallization, increase the dissolution rate	(Warwick et al., 2002)
Curcumin	Acetone, Ethanol, Acetonitrile, Methanol	20 mL/min	1–10 mg/mL	25–40	9.5–10	–	Comparison of GAS and ARISE, scale up	(Kurniawansyah et al., 2017)
Finasteride	DMSO	–	10, 25, 40 mg/mL	35–55	10, 13, 16	333.56–1432.9 nm	Particle size reduction	(Najafi 2021)
5-Fluorouracil	DMSO	1.6, 2, 2.4 mL/min	20, 60, 100 mg/mL	34, 40, 46	9, 12, 15	260–600 µm	Particle size reduction	(Esfandiari 2013)
5-Fluorouracil + nanoclay	Methanol	20 mL/min	–	25	12	–	Drug release measurement	(Harikrishnan et al., 2020)
Gastroresitant	Acetone, DMSO	0.1–0.2 bar/min	–	40	9.5	1–2 µm	Comparison GAS, ASES, and ARISE	(Tandya et al., 2016)
Ginkgo-ginkgolides	Ethanol	0.8 Kg/hr	0.1–0.3	25–45	9–18	0.8–240 µm	Particle size reduction	(Chen 2005)
Griseofulvin	Dimethylformamide	–	0.1–1 %	25	4–6	0.5–500 µm	Comparison of two different micro mixer	(Arora et al., 2020)
Ibuprofen + R-phenylethylamine	Methanol, Ethanol	–	–	45	10, 15, 20	1–3 µm	Cocrystallization,	(Lőrincz et al., 2016)
Insulin	DMSO, DMFA	0.57 bar/min	5, 15 mg/mL	25–35	8.6	90 % < 4 µm 10 % < 1 µm	Particle size reduction	(Yeo et al., 1993)
Itraconazole/L/maliacid	THF	1 g/min	25 mg/mL	40	10.3	–	Cocrystallization, increase the dissolution rate	(Ober et al., 2013)
Ketoconazole-4-aminobenzoic acid	Methanol, Ethanol, Acetone	10 mL/min	–	25–45	9	12.88–14 µm	Cocrystallization, dissolution rate determine	(Kotbantao and Charoenchaitrakool 2017)

**Table 2** (continued)

Pharmaceutical compound	Solvent	Antisolvent Addition Rate	Initial solute concentration	Temperature (°C)	Pressure (MPa)	Mean particle size	Objective of micronizing	Ref
Levothyroxine sodium	Ethanol	20 mL/min	2–4 mg/mL	25–50	9–12	370–500 µm	Comparison GAS and ARISE, particle size reduction	(de Melo et al., 2014)
Liposome	Ethanol, Chloroform			40–65	5–20	0.1–10 µm	Particle size distribution, stability study	(Shashidhar 2016)
Mefenamic acid + Paracetamol	Acetone	10 mL/min	–	25–45	9	1–350 µm	Cocrystallization, dissolution study	(Wichianphong and Charoenchaitrakool 2018)
Mefenamic acid + Polyvinylpyrrolidone	Acetone, Ethanol	10 mL/min	–	25, 35	9	–	Dissolution rate increased	(Dittanet et al., 2016)
Naproxen + nicotinamide	Acetone	25 g/min	–	35	10	< 180 µm	Cocrystallization, dissolution rate increased	(Neurohr et al., 2013)
Naproxen + nicotinamide	Acetone	–	–	20–60	8–20	–	Cocrystallization, solubility increased	(Revelli et al., 2014)
Naproxen + nicotinamide	Acetone	2, 3 g/min	50, 120 mg/mL	37	10	40–80 µm	Cocrystallization, kinetics modeling cocrystallization	(Erriguible et al., 2015)
Paclitaxel	DMSO	1–3 mL/min	5–10 %	50	10–20	82–131 nm	drug loading efficiency controlled	(Ghoreishi 2017)
Paracetamol	Ethanol, TEO	0.3 mL/min	–	40	9	–	Dug deliver and loading study	(Ulker and Erkey 2017)
Paracetamol	Acetone	0.067–6 L/min	0.5–0.9 g/L	5–40	–	5–250 µm		(Fusaro et al., 2004)
Phenanthrene	Toluene	1–100 mL/min	25–100 %	25–65	–	21.2–209.9 µm	Smaller particle size, narrow size distribution	(Bakbakhhi et al., 2005)
Pol( $\epsilon$ -Caprolactone)	Acetone	10 mL/min		35	10, 12, 14	53–135 µm	Encapsulation efficiency, in vitro release study	(Sakata 2021)
Posaconazole + 4aminobenzoic acid	Acetonitrile	46 g/min	10.4 mg/mL	35, 65	10, 20	20–43 µm	Cocrystallization, comparison of GAS and CSS	(Long et al., 2021)
Puerarin	Ethanol, Aceton, Methanol	25 mL/min	60–120 mg/mL	30–43	8–14	29.7–49.26 µm	Particle size reduction	(Li et al., 2016)
Rosuvastatin	DMSO		20–60 mg/mL	40–65	10.5–18	63.2–156.4 nm	Particle size reduction	(Najafi 2021)
Sertraline hydrochloride	DMSO	3 g/min	10, 35, 60 mg/mL	35–55	10–20	102–500 µm	Comparison RESS-SC and GAS, dissolution rate study	(Sodeifian et al., 2022)
Sulfamethoxazole-Poly (vinylpyrrolidone)	Acetone, Methanol, Ethanol	10 mL/min	25, 50, 75 %	34, 40, 45	9	57–266 µm	Dissolution rate enhancement	(Phothipanyakun et al., 2013)
Theophylline	Methylene chloride, Ethanol	0.2–2 MPa/min	12–32 mg/mL	25–50	6.5–10	10–150 µm	Particle size distribution, comparison SAS and GAS	(Roy et al., 2011)

**Table 3** The result of capecitabine nanoparticle production via Box-Behnken design (Amani 2021).

Run	Pressure (bar)	Initial solute concentration (mg/mL)	Temperature (K)	Particle size (nm)
1	140	75	328	868.8
2	140	15	308	332.8
3	140	75	308	468.2
4	120	75	318	758.1
5	120	45	328	1090.9
6	160	75	318	498.3
7	120	15	318	639.9
8	140	45	318	576.9
9	140	45	318	540.6
10	140	45	318	534
11	160	45	328	567.8
12	140	45	308	263.7
13	140	15	328	662
14	120	45	308	534.4
15	140	45	318	542.9
16	160	15	318	243.3
17	140	45	318	521.4

**Table 4** The mean particle size of phenanthrene production via the GAS process at different carbon dioxide addition rates (Bakbakhhi et al., 2005).

Carbon dioxide addition rate (mL/min)	Mean particle size ( $\mu\text{m}$ )
1	177.5
20	85.7
50	46.1
100	25.1

**Table 5** Effect of initial solute concentration on sertraline hydrochloride particle size (Sodeifian et al., 2022).

Pressure (bar)	Temperature (K)	Initial solute concentration (mg/mL)	Mean particle size (nm)
200	328	10	113
200	328	60	233
150	338	10	311
150	338	60	408

## 2. Gas antisolvent process

Gallagher et al. (1989) investigated the GAS process for the first time. Then, the crystallization of an organic salt for pharmaceutical application with the GAS method was studied (Amaro-González 2000). Nanosphere of Insulin and Insulin-PEG-PLA were produced by the GAS process (Elvassore et al., 2001). In the past few decades, the use of the GAS method for the production of pharmaceutical nanoparticles has been highly considered. The supercritical fluids act as an antisolvent in the GAS process. To prepare nanoparticles by employing this technique, the solute is first dissolved in a solvent, a specific amount of which is poured into a cell. This cell is placed in an oven for controlling temperature, to which supercritical fluid is injected, leading to the deposition of solute

particles with a new particle size distribution on the filter at the end of the cell. The equipment applied to produce nanoparticles by using supercritical carbon dioxide is depicted in Fig. 3. Briefly, carbon dioxide passes through a molecular sieve to remove impurity and moisture, and its temperature is diminished by using a cooler to liquefy so that its pressure can promote by using an HPLC pump. Furthermore, the carbon dioxide with an increased pressure passes through a rotary heat exchanger inside the oven with an intended temperature for raising its temperature, followed by entering into a cell. The pressure between the pump with the end of the cell is controlled by using a back pressure valve. Finally, the particles precipitated on the filter at the end of the cell are collected (Esfandiari 2013).

### 2.1. Experimental

The GAS technique has been employed to assess the production of a wide range of nanoparticles. Table 2 outlines solvent, antisolvent addition rate, temperature, pressure range, and particle size, as well as the type of substance and initial concentration of solute. In each of the studies, the effect of these parameters on particle size and particle size distribution has been investigated. In some cases, the amount of solubility has been studied. The main objective of reducing the size of pharmaceutical particles is to increase the ability of dissolution and biological absorption and reduce the used dosage.

#### 2.1.1. Effect of pressure

An elevation in pressure leads to a smaller particle. The particle deposition using the GAS process is caused by the volume expansion of the solution (solute in solvent) after adding antisolvent, mostly supercritical carbon dioxide, into the organic solvent. Following a rise in pressure, carbon dioxide density enhances, and consequently its solubility increases in the organic solvent. Thus, a shorter time is required to reach supersaturation and precipitation. Indeed, the nucleation mechanism is dominant at greater pressure, which results in producing many small particles. Fig. 4 completes the descrip-

**Table 6** The effect of solvent on particle size production of aspirin via GAS (Jafari et al., 2015).

Antisolvent addition rate (bar/min)	Temperature (°C)	Initial aspirin concentration (g aspirin/g solution)	Solvent	Mean particle size (µm)
8	42	0.2	Acetone	114
8	42	0.2	Methanol	71
40	37	0.27	Acetone	94
40	37	0.27	Methanol	59
8	37	0.2	Acetone	101
8	37	0.2	Methanol	67
40	42	0.2	Acetone	71
40	42	0.2	Methanol	59
8	37	0.27	Acetone	122
8	37	0.27	Methanol	72
8	42	0.27	Acetone	124
8	42	0.27	Methanol	78
40	42	0.27	Acetone	98
40	42	0.27	Methanol	63

**Table 7** Effect of solvent on the minimum pressure of the ternary system (CO<sub>2</sub>, solvent, ampicillin) (Rahmanzadeh Derisi 2020).

Solvent	M <sub>w</sub>	P <sub>min</sub> (MPa)
Ethanol	46.06	7.88
1-propanol	60.09	8
1-butanol	74.12	8.05
1-pentanol	88.15	8.18

tion above (Sodeifian et al., 2022). Accordingly, a lower amount of supersaturation is spent on particle growth. Such a trend has been reported in preparing the nanoparticles of basil seed mucilage (Ghoreishi 2017), ibuprofen (Lórinz et al., 2016), ampicillin (Esfandiari 2015), and 5-Fluorouracil

(5-FU) (Esfandiari 2013), capecitabine (Amani 2021), finasteride (Najafi 2021). Fig. 5a and b demonstrate the 5-FU nanoparticles synthesized through applying the GAS method at 12 and 15 MPa, respectively. The other operating conditions such as temperature and carbon dioxide injection rate, as well as the initial concentration of solute, are the same in both experiments. Based on the results, smaller nanoparticles are produced by elevating pressure (Esfandiari 2013). Amani et al. used Box-Benken for experimental design to produce capecitabine nanoparticles via the GAS process. The average particle size obtained under different conditions was given in Table 3 (Amani 2021).

### 2.1.2. Effect of temperature

The results of the studies on nanoparticle preparation through employing the GAS technique revealed an improvement in

**Table 8** Modeling of different ternary systems including carbon dioxide as an antisolvent, solvent, and solute.

System (antisolvent, solvent, solute)	Equation of state	Mixing Rule	Temperature range (K)	Minimum pressure (MPa)	Ref
CO <sub>2</sub> -DMSO-ampicillin	PR	Vidal and Michelson	308, 313, 319	7.3, 8, 8.97	(Esfandiari 2015)
CO <sub>2</sub> -DMSO-finasteride	PR	van der Waals	308, 318, 328, 338	7.49, 8.13, 8.51, 9.03	(Najafi 2020)
CO <sub>2</sub> -methanol-carbamazepine	PR	van der Waals	313, 343		(Muthancheri et al., 2020)
CO <sub>2</sub> , ethanol, ampicillin	PR	Vidal and Michelson	308.15, 310.15, 313.15	7, 7.29, 7.88	(Rahmanzadeh Derisi 2020)
CO <sub>2</sub> , 1-propanol, ampicillin	PR	Vidal and Michelson	308.15, 313.15, 316.15	7.08, 8, 8.74	(Rahmanzadeh Derisi 2020)
CO <sub>2</sub> , 1-butanol, ampicillin	PR	Vidal and Michelson	308.15, 313.15, 316.15	7.18, 8.05, 8.18	(Rahmanzadeh Derisi 2020)
CO <sub>2</sub> , 1-pentanol, ampicillin	PR	Vidal and Michelson	308.15, 313.15, 316.15	7.3, 8.18, 8.81	(Rahmanzadeh Derisi 2020)
CO <sub>2</sub> , DMSO, Capecitabine	PR	van der Waals	308, 318, 328, 338	7.80, 8.57, 9.78, 10.46	(2021)
CO <sub>2</sub> , DMSO, Capecitabine	SRK	van der Waals	308, 318, 328, 338	7.27, 7.61, 7.95, 8.13	(Amani 2021)
CO <sub>2</sub> , ethanol, Atenolol	PR	van der Waals	313		(Kikic et al., 1997)
CO <sub>2</sub> + dichloromethane + medroxyprogesterone	PR	van der Waals	303, 313, 323, 333	7, 7.9, 8.5, 9.3	(Giufriada et al., 2014)

**Table 9** Kinetic parameters of different pharmaceuticals precipitation via the GAS process.

System	Antisolvent addition rate	$\alpha''$ (dimensionless)	$K_g$ (m/s)	$g$ (dimensionless)	$B'$ ( $\#/m^3 s^1$ )	$B''$ ( $\#/m^3 s^1$ )	Ref
CO <sub>2</sub> , toluene, phenanthrene	1 (mL/min)	$8.11 \times 10^{-17}$	$4.49 \times 10^{-5}$	1.87	$8.9 \times 10^5$	$5.8 \times 10^6$	(Bakbakhhi et al., 2005)
	50				$8 \times 10^{10}$	$4.9 \times 10^9$	
	100				$9.9 \times 10^{12}$	$1.5 \times 10^9$	
CO <sub>2</sub> , DMSO, 5-Fluorouracil	1.6 (mL/min)	$5.5201 \times 10^{-18}$	$5.6417 \times 10^{-9}$	1.4512	$8.6 \times 10^{27}$	$2.1 \times 10^{24}$	(Esfandiari 2014)
	2	$7.5361 \times 10^{-18}$	$5.1204 \times 10^{-9}$	1.4338	$9 \times 10^{27}$	$3.5 \times 10^{24}$	
	2.4	$9.6568 \times 10^{-18}$	$5.9007 \times 10^{-9}$	1.4282	$9.6 \times 10^{27}$	$4.6 \times 10^{24}$	
CO <sub>2</sub> , DMSO, Ampicillin	1.6 (mL/min)	$5.6481 \times 10^{-13}$	$5.8484 \times 10^{-10}$	1.6255	$2.84 \times 10^{28}$	$2.13 \times 10^{28}$	(Esfandiari 2013)
	2	$5.75 \times 10^{-13}$	$5.8421 \times 10^{-10}$	1.6233	$2.9 \times 10^{28}$	$2.3 \times 10^{28}$	
	2.4	$5.2412 \times 10^{-13}$	$5.6241 \times 10^{-10}$	1.6187	$3.33 \times 10^{28}$	$2.8 \times 10^{28}$	
CO <sub>2</sub> , acetone, BDP	25 (mL/min)	$2.114 \times 10^{-15}$	$2.645 \times 10^{-6}$	2.184			(Dodds 2007)
	50	$2.313 \times 10^{-15}$	$2.574 \times 10^{-6}$	2.17			
CO <sub>2</sub> , acetone, aspirin	8 (bar/min)	$4 \times 10^{-23}$	$8 \times 10^{-6}$	2	$1 \times 10^7$	$6 \times 10^8$	(Jafari 2017)
	40 (bar/min)				$7 \times 10^{10}$	$8 \times 10^9$	
CO <sub>2</sub> , methanol, aspirin	8 (bar/min)	$10^{-24}$	$0.9 \times 10^{-6}$	1.55	$8 \times 10^7$	$5 \times 10^8$	(Jafari 2017)
	40 (bar/min)				$5 \times 10^{10}$	$9 \times 10^8$	
CO <sub>2</sub> , toluene, phenanthrene	1 (mL/min)	$6.49 \times 10^{-17}$	$5.18 \times 10^{-5}$	1.69	$1 \times 10^6$	$9 \times 10^6$	(Bakbakhhi 2009)
	20				$2 \times 10^7$	$7 \times 10^7$	
	50				$9 \times 10^{10}$	$3 \times 10^8$	
	100				$9.2 \times 10^{12}$	$1.3 \times 10^9$	

$\alpha''$ : Secondary nucleation rate coefficient,  $K_g$ : Growth rate coefficient,  $B'$ : Primary nucleation rate,  $B''$ : Secondary nucleation rate,

**Table 10** The advantage and disadvantage of supercritical fluid method to production nanoparticles.

Method	Advantage	Disadvantage	Limitation
RESS	-No conventional solvent -Scale up easy -Low/mild processing temperature -Formation of nanoparticles is possible	-Broad particle size distributions -High pre-expansion pressure	-For encapsulation, pharmaceutical and the coating material are dissolved in the SCF, but many pharmaceutical has low solubility in SC-CO <sub>2</sub>
GAS	- Simple - Particularly useful -Low/mild processing temperature -solvent and CO <sub>2</sub> can be recovered -Formation of nanoparticles is possible -Narrow size distributions	- Batch mode - Small production capacity	-Low volume of precipitation vessel
SAS	-Continues -Large scale mass production -Low/mild processing temperature -Formation of nanoparticles is possible	-Particle agglomeration if not immediately worked-up - stabilizers may be needed for stabilization	
SEDS	-Improve mass transfer between SC-CO <sub>2</sub> and droplets -Formation of nanoparticles is possible		
ASES	-ASES can be produced high drug loading with less solvent residues		-mass transfer processes
PGSS	-Can operate either batch or continuously - easy scale-up -mild operating conditions - homogenous products	- Difficult to control particle sizes	

particle size after promoting temperature. The higher temperature reduces the solubility of carbon dioxide in an organic solvent, along with increasing that of solute particles in a solvent. In general, diminution is found in volume expansion and

nucleation, fewer nuclei are synthesized, and growth is considered the dominant mechanism. Regarding 5-FU nanoparticle production by using the GAS process, the mean size is 400, 480, and 600 nm at 34, 40, and 46°C, respectively, by assuming

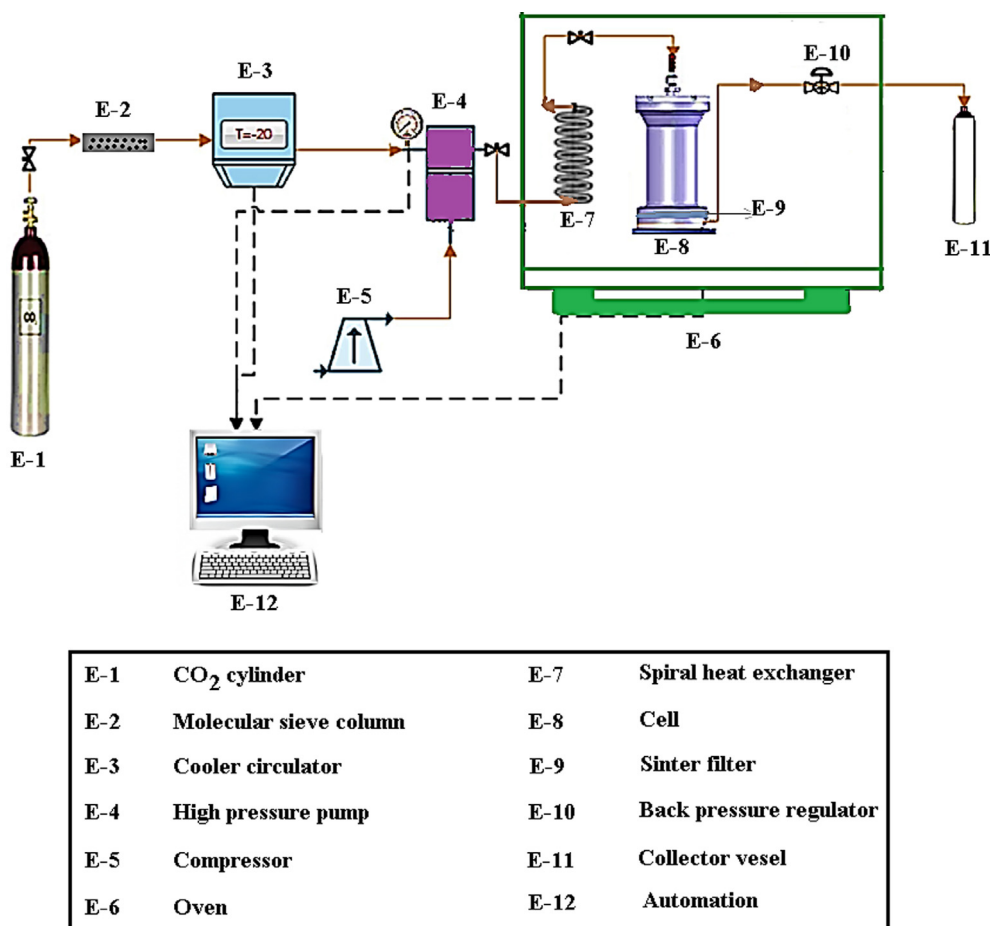


Fig. 3 Process flow diagram of GAS experimental apparatus.

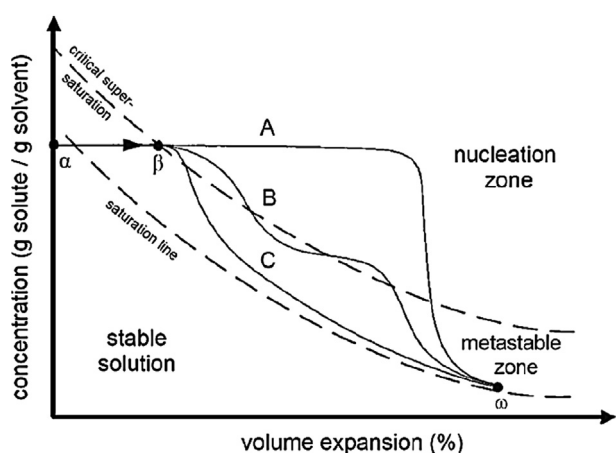


Fig. 4 A conceptual model for describing the nucleation and growth mechanism of the GAS process (Muller et al., 2000).

the constancy of other parameters (pressure, antisolvent addition rate, and initial concentration of solute) (Esfandiari 2013). Fig. 6 shows the size of finasteride particles by changing the temperature. As is evident in Fig. 6, at constant pressure with increasing temperature the particle size has grown larger (Najafi 2021). Comparison of run results 1 and 3 in Table 3 for

particle production of capecitabine with the gas antisolvent process, shows that the particle size increases as the temperature increases. The reason for this event is the dominating of the growth rate at higher temperatures (Amani 2021). This elevation in particle size at greater temperature is consistent with the results of other research about nanoparticle preparation according to the GAS technique (Cocero and Ferrero 2002, Fusaro et al., 2004, Bakhbakhi et al., 2006, Esfandiari 2015, Jafari et al., 2015, Li et al., 2016, Amani 2021, Najafi 2021, Sodeifian et al., 2022).

### 2.1.3. Effect of antisolvent injection rate

Some researchers evaluated the mean and distribution of ampicillin particle size at the three antisolvent addition rates of 1.6, 2, and 2.4 mL/min by considering the constant temperature of 40°C, pressure of 12 MPa, and initial concentration of 60 mg/mL. The results indicated a decrease in the mean particle size following an enhancement in the antisolvent addition rate. Adding a higher value of antisolvent leads to a greater level of volume expansion, supersaturation, dominance of the nucleation mechanism, and a large number of initial nuclei. A significant amount of supersaturation is consumed for nucleation, and consequently, the particles grow less. The mean particle size results of phenanthrene produced by the GAS method in different supercritical carbon dioxide addition rates have been reported in Table 4. The results show that with increasing the

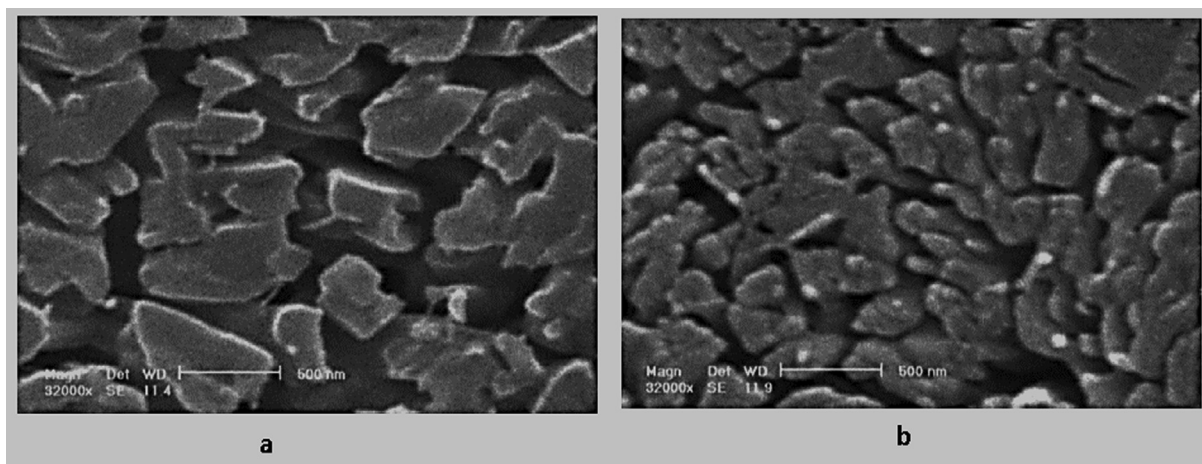


**Fig. 5** SEM image of 5-Fluorouracil obtained by GAS process at 34°C, the CO<sub>2</sub> flow rate of 2 mL/min, initial solute concentration 60 mg/mL, and (a) pressure 12 MPa, (b) Pressure 15 MPa (Esfandiari 2013).

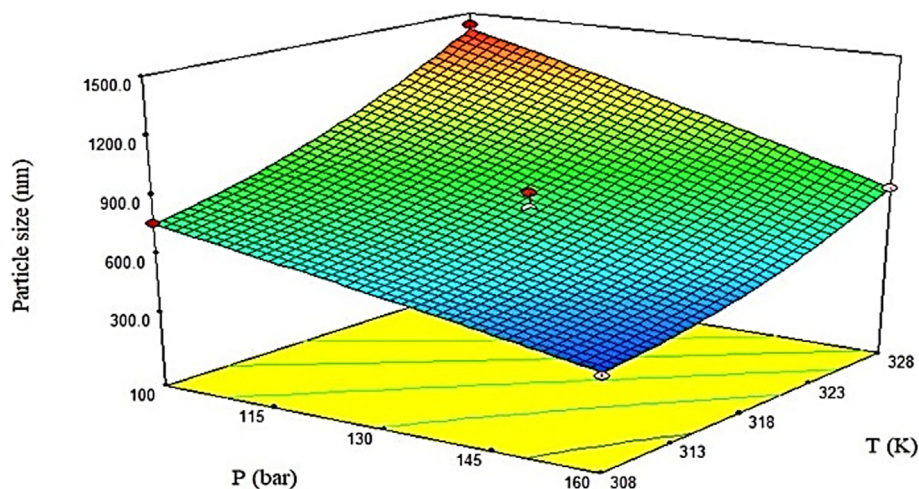


**Fig. 6** The influence of temperature and pressure on the particle size of finasteride (Najafi 2021).

supercritical carbon dioxide addition rate, the particle size has decreased (Bakbakhhi et al., 2005). The results are in line with those reported by some researchers (Fusaro et al., 2004, Bakbakhhi et al., 2006, Esfandiari 2015, Jafari et al., 2015). To better explain the process of its relationship the solubility and volumetric expansion are defined. The particle deposition using the GAS process is caused by the volume expansion of the solution (solute in solvent) after adding antisolvent, mostly supercritical carbon dioxide, into the organic solvent. Fig. 4 shows the solubility reduction with the volumetric expansion of the solution. The plan is divided into three zones (stable solution, metastable, and nucleation) by saturation and critical supersaturation line. In the GAS process, the solution is first located below the saturation point, i.e. at point  $\alpha$ . Nucleation can happen at points  $\alpha$  and  $\beta$ . Between these two points  $\alpha$  and  $\beta$ , there are two processes in competition: supersaturation increase with increasing carbon dioxide, and supersaturation decrease as a result of nucleation. In this Figure, curves A and C are plotted for two different speeds of carbon dioxide

addition rate as an antisolvent. In the high speed of antisolvent addition rate (Cure A) due to high supersaturation, the rate of nucleation increases. It produces a large number of nuclei and a large amount of supersaturation is consumed below the critical supersaturation line. So less growth happens. At the low speed of antisolvent addition (Cure C), as soon as supersaturation is created nucleation happens at the lower point of  $\beta$ . So there are fewer nuclei than the previous case (Cure A), which can grow and create larger particles (Muller et al., 2000).

#### 2.1.4. Effect of initial solute concentration

At the higher initial concentration, the supersaturation profile is closer to the saturation line and nucleation occurs in lower expandability. Therefore, the resultant nuclei possess more opportunities to grow and the growth mechanism dominates. Accordingly, a rise in the initial concentration of solute in organic solvent elevates the mean particle size in the GAS method. Fig. 7 a and b show the finasteride particles produced by the gas process at the same temperature and pressure and

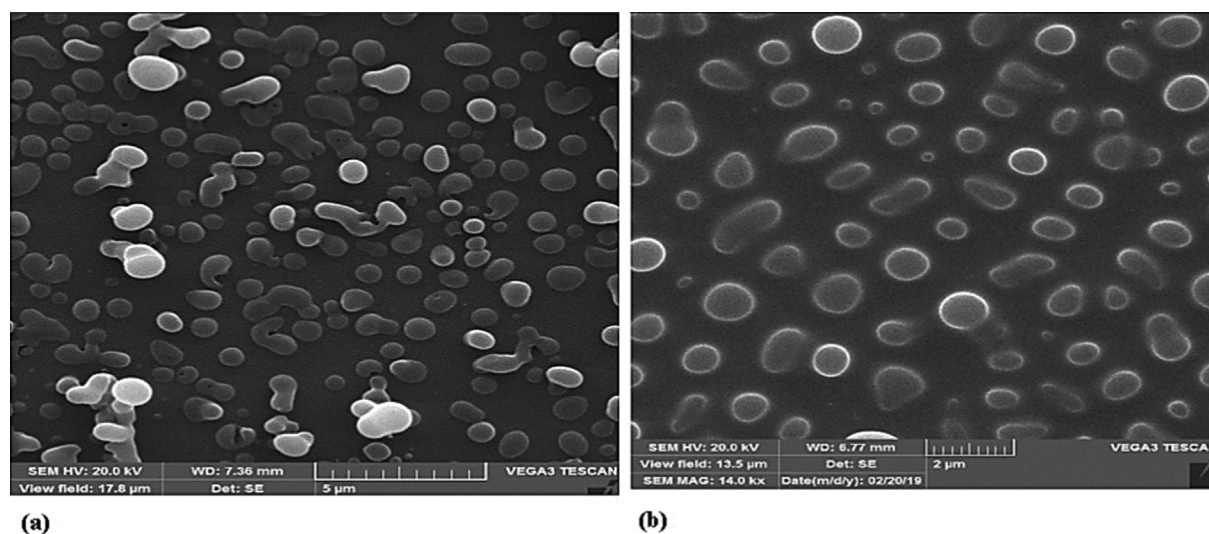


**Fig. 7** SEM images of produced finasteride by a GAS process (13 MPa, 35 °C) at various initial solute concentration (a)10 and (b)40 mg/mL (Najafi 2021).

the initial concentrations of 10 and 40 mg/mL. According to Fig. 7 a and b, the particle size increased with the increase in initial concentration (Najafi 2021). According to Table 3, an increase in the initial concentration of capecitabine increases at a constant pressure of 140 bar and temperature of 328 K the capecitabine particle size from 662 nm to 868.8 nm (Amani 2021). At the same temperature and pressure, the effect of increasing the initial concentration on the size of sertraline hydrochloride particles produced by the GAS process has been investigated. The results in Table 5 show that with increasing the initial concentration, the particle size increases (Sodeifian et al., 2022). Based on Fig. 4, at higher initial concentrations, the primary nuclei are produced at low expansion volumes and have a higher growth opportunity. This trend is in agreement with the results of some other studies (Fusaro et al., 2004, Bakhbakhi et al., 2006, Esfandiari 2013, Esfandiari 2015, Jafari et al., 2015, Ardestani 2021, Najafi 2021, Sodeifian et al., 2022).

### 2.1.5. Effect of solvent

Cocero and Ferrero compared the volume expansion of ethyl acetate and dichloromethane solvents by adding carbon dioxide. They found a higher expansion in the dichloromethane and no difference in crystal size and its distribution in the presence of the two solvents (Cocero and Ferrero 2002). Following the use of *N*-methyl pyrrolidone (NMP) and dimethyl sulfoxide (DMSO) solvents, a change is observed in the shape of copper indomethacin nanoparticles (Warwick et al., 2002). An approximate comparison of the particle size using the SEM image was shown that the particles produced by NMP are larger than DMSO. The molecular weight of NMP and DMSO are 99.133 and 78.13, respectively. Bakhbakhi et al. examined the effect of methanol, ethanol, and acetone as a solvent on producing beclomethasone-17,21-dipropionate (BECD) nanoparticles based on the GAS technique. Based on the results, powder particles with lower crystallinity and needle-like crystals with higher crystallinity are prepared after utilizing methanol and ethanol, respectively (Bakhbakhi et al.,

2006). Additionally, the aspirin nanoparticles deposited with acetone exhibit a greater degree of crystallinity in comparison with those precipitated in the presence of methanol. In the constant condition of the addition of antisolvent, temperature, and initial aspirin concentration, the particle size for two solvents acetone and methanol has been compared in Table 6 (Jafari et al., 2015). The results show that in all cases the particle size obtained by methanol is smaller than the particle size obtained by acetone. The molecular weight of methanol (32.04 g/mol) is less than acetone (58.08 g/mol). In the study of ampicillin modeling produced by GAS method with different solvents, it can be seen that solvent with lower molecular weight shows less minimum pressure and it is expected that particles with smaller mean size will be created (Rahmanzadeh Derisi 2020). The effect of solvent molecular weight on particle size is consistent in these two studies. The mean particle size of puerarin is minimized by applying ethanol. The methanol solvent results in obtaining dense prism-shaped and long needle-like powders, while less dense needle-like powders with many dents and more crystallinity are synthesized following the addition of acetone (Li et al., 2016). Research has shown that entering solvent molecules into the solid lattice or interaction between solvents and growing crystals alters the morphology of particles (Muller et al., 2000). Volumetric expansion directly affects supersaturation. Therefore, it is effective on the crystals produced. Different solvents have different equilibrium conditions to achieve volumetric expansion. Therefore, it is expected to create different crystalline particles with different solvents under the same conditions (Cocero and Ferrero 2002).

### 2.2. Thermodynamic modeling

No particle precipitations have been detected in GAS under any operational conditions. The appropriate condition to achieve the reasonable applicability of the GAS process can be determined by thermodynamic modeling. The GAS process is based on the pressurization of a liquid solution by gas to

dissolve it in the liquid phases thus resulting in the solute precipitation from the solution. Upon the injection of supercritical carbon dioxide into the solution, the volumetric features of the solution will alter by the prompt volume expansion. Therefore, the selection of a suitable solvent in the GAS process is highly important to determine the exact volumetric behavior of the solution at high CO<sub>2</sub> pressures. For calculation of the operation pressure, the relative molar volume was estimated. Fuente Badilla et al. evaluated thermodynamic modeling and volume expansion relation for binary and ternary component mixtures (de la Fuente Badilla et al., 2000).

$$\frac{\Delta V}{V} = \frac{V(T, P) - V_0(T, P_0)}{V_0(T, P_0)} \quad (1)$$

Where,  $v(T, P)$  represents the liquid phase molar volume at a given temperature and the pressure, while  $v_0(T, P_0)$  stands for the solvent molar volume at the system temperature and reference pressure of  $P_0$  ( $P_0 = 101.325$  kPa). Some other researchers applied the Peng-Robinson (PR) equation of state to examine the thermodynamic modeling of the systems toluene, phenanthrene, carbon dioxide, and determined the interaction parameters of the components (Muhrrer et al., 2002). Additionally, the proper temperature and pressure range for producing ampicillin nanoparticles according to the GAS method was specified through modeling the carbon dioxide-DMSO-ampicillin ternary system thermodynamically. Based on the results of modeling, an increase occurred in the minimum pressure by elevating temperature. The calculated  $P_{\min}$  was 7.3, 8, and 8.97 MPa at 308, 313, and 319 K (Esfandiari 2015). The thermodynamic modeling was applied to evaluate liquid–solid phase behavior during the crystallization of carbamazepine by utilizing the GAS process in the presence of carbon dioxide and methanol as antisolvent and solvent, respectively (Muthancheri et al., 2020). Fig. 8 shows the variations of the relative molar volume of the liquid phase in terms of pressure for the binary system (CO<sub>2</sub>-DMSO) at 328 K. As can be seen, by pressure enhancement, the volume expansion first decreased and exhibited a minimum at 7.95 MPa followed by a sharp increase. Therefore, the operating pressure in this system is greater than  $P_{\min}$  (7.95 MPa). The volume of the liquid phase in terms of pressure for the binary system (CO<sub>2</sub>-DMSO) at 328 K. As can be seen, by pressure enhancement, the volume expansion first decreased and

exhibited a minimum at 7.95 MPa followed by a sharp increase. Therefore, the operating pressure in this system is greater than  $P_{\min}$  (7.95 MPa).  $P_{\min}$  of the ternary system was higher than that of the binary system at a constant temperature, reflecting the significance of calculating the optimal operating conditions in the ternary system (Esfandiari 2015).

An experiment system was designed for synthesizing finasteride nanoparticles by using the GAS technique after determining the allowed temperature and pressure through modeling carbon dioxide-DMSO binary and carbon dioxide-DMSO-finasteride ternary systems thermodynamically. Fig. 9 shows the relative molar volume change–pressure curve for ternary system carbon dioxide-DMSO-finasteride. As indicated the minimum value of pressure increased by temperature. The calculated  $P_{\min}$  were 7.49, 8.13, 8.51, and 9.03 MPa at 308, 318, 328, and 338 K, respectively (Najafi 2020). Some researchers investigated the effect of various alcoholic solvents on the thermodynamic modeling of the carbon dioxide-solvent-ampicillin ternary system in the GAS process. They found a greater minimum pressure following an improvement in solvent molecular weight (Table 7) (Rahmanzadeh Derisi 2020). To determine interaction parameters and minimum pressure, the behavior of the phase equation of carbon dioxide-DMSO-capecitabine ternary system as an anticancer drug was modeled to obtain the pressure and temperature range desired for the precipitation experiments of capecitabine based on the GAS method. In this respect, the PR and SRK equations of state were applied for modeling (Amani 2021). Modeling of different ternary systems including carbon dioxide as an antisolvent, solvent and solute were reviewed in Table 8.

### 2.3. Kinetic modeling

The control of particle size and particle size distribution is important for pharmaceuticals. Achieving particles with specific particle size distribution requires an understanding of the particle formation mechanism. By investigating the kinetic modeling of the crystallization process of pharmaceutical nanoparticles called the gas solvent, the behavior of the system will be determined.

In the GAS process, the solute is dissolved in an organic solvent. The solution is expanded by supercritical carbon dioxide as an antisolvent. Then, the particles are precipitated via

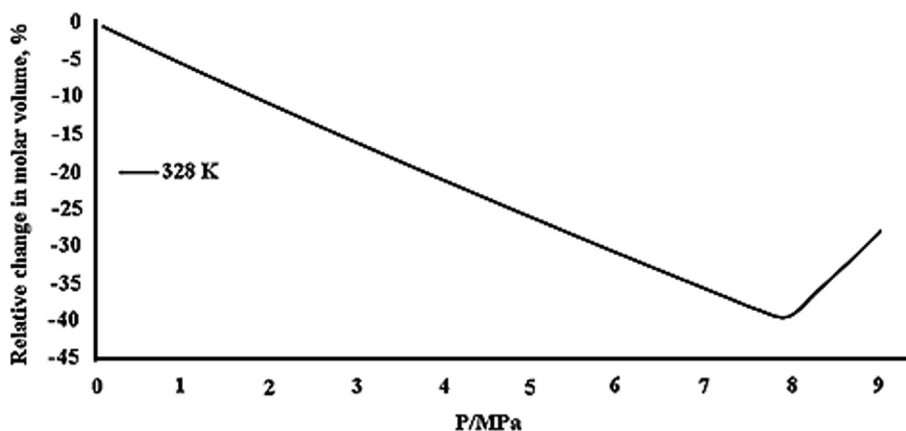
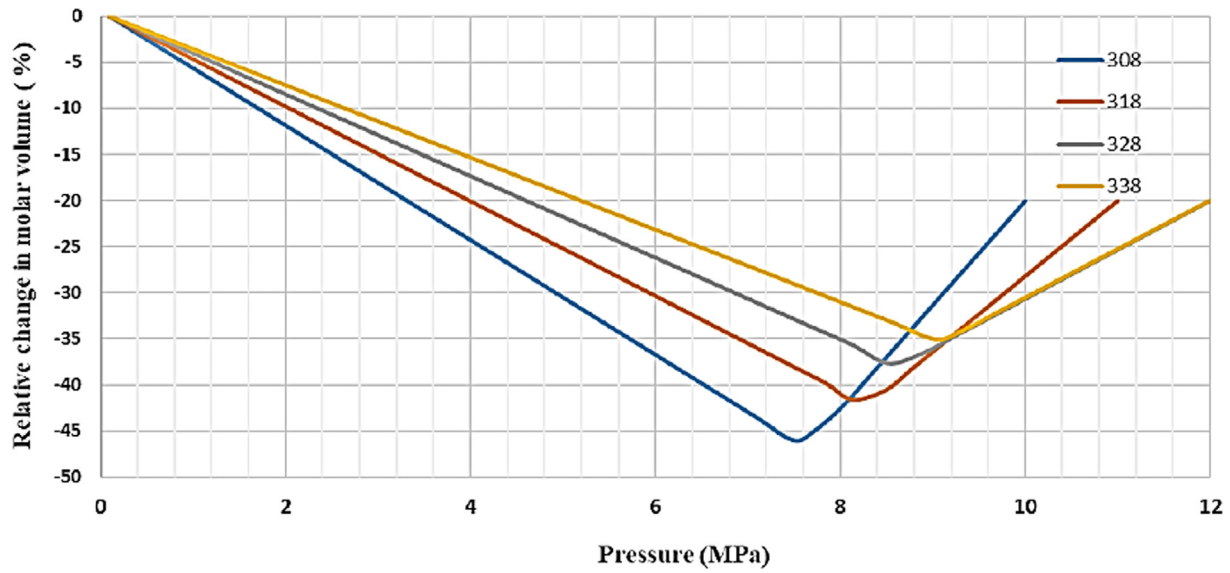


Fig. 8 Relative expansion of the liquid phase as a function of pressure, calculated according to PR for the systems DMSO–CO<sub>2</sub> at 328 K (Esfandiari 2015).



**Fig. 9** Relative expansion of the liquid phase as a function of pressure for the system CO<sub>2</sub>-DMSO- finasteride at different temperatures (308, 318, 328, 338 K) (Najafi 2020).

nucleation and growth mechanisms. The primary nucleation occurs at the beginning of the GAS process. The remaining supersaturation is spent on nuclei growth. Secondary nucleation occurs due to particles colliding with each other and hitting the cell wall. In order to kinetic modeling, population and mass balance equations were written. Initial condition, boundary condition, and numerical solution method of partial equations were determined. The objective function, which is the difference between the cumulative density obtained from the model and the experiment, was considered. The initial parameters of growth rate and nucleation are guessed. In the first period, supersaturation, nucleation rate, and boundary conditions are obtained. Population density is calculated in the next time interval.

Where  $B$  is the nucleation rate. That's the sum of primary nucleation  $B'$  and secondary nucleation  $B''$ , which are given as follows (Dodds et al., 2007; Muhrer et al., 2002; Bakhbakhi et al., 2005):

$$B = B' + B'' \quad (2)$$

$$B' = 1.5D(c_p N_A)^{7/3} \sqrt{\frac{\gamma}{kT}} \times \frac{v_p}{N_A} \exp\left[-\frac{16\pi}{3} \left(\frac{\gamma}{kT}\right)^3 \left(\frac{v_p}{N_A}\right)^2 \left(\frac{1}{\ln S}\right)^2\right] \quad (3)$$

$$B'' = \frac{\alpha'' a_v D}{d_M^4} \exp\left[-\pi \left(\frac{\gamma d_M^2}{kT}\right)^2 \frac{1}{\ln S}\right] \quad (4)$$

$$c_p = \frac{x_p}{v_L} \quad (5)$$

$$\gamma = 0.414kT(c_p^S N_A)^{2/3} \ln\left(\frac{c_p^S}{c_p}\right) \quad (6)$$

$$a_v = k_a m_2 \quad (7)$$

$$D = \frac{kT}{2\pi\eta d_M} \quad (8)$$

$$d_M = \sqrt[3]{\frac{v_p}{N_A}} \quad (9)$$

$$S = \frac{f_p^L}{f_p^S} \quad (10)$$

The particle growth rate,  $G$ , is calculated by (Muhrer et al., 2002):

$$G = k_g (S - 1)^g; \quad (11)$$

The  $\alpha''$ ,  $k_g$ , and  $g$  were secondary nucleation rate coefficient, growth rate coefficient, and growth rate order with respect to supersaturation, respectively. The value of kinetic parameters, primary and secondary nucleation of different pharmaceuticals precipitation via the GAS process were obtained at different antisolvent addition rates in Table 9. Kinetic modeling was implemented in various studies. For example, the nucleation and growth rate of phenanthrene nanoparticles was specified by examining the kinetic modeling of their products according to the GAS method (Bakhbakhi et al., 2005). Some researchers studied the kinetic modeling for preparing carbamazepine nanoparticles according to the GAS technique (Muthancheri et al., 2020).

The kinetic model for preparing the nanoparticles of beclomethasone 17, 21-dipropionate through using the GAS technique was studied by considering acetone as solvent and carbon dioxide as antisolvent. In this regard, modeling was performed by using the PR equation of state (Dodds 2007). Further, ampicillin nanoparticles were kinetically modeled to obtain nucleation and growth rate. The PR equation of state was used to calculate liquid phase fugacity and DMSO was applied as solvent. Population and material balance equations were used to determine growth and nucleation rate. The combination of the Crank-Nicholson and Lax-Wendroff methods

were used in this modeling. This method is used as a highly efficient numerical algorithm for solving a stationary partial differential equation with time discretization. The expanded Taylor-series mixed with explicit finite difference methods makes the Lax-Wendroff method. But the Crank-Nicholson method is based on a limited implicit difference. The Lax-Wendroff/Crank-Nicholson mixture method can be used to crystallization and does not require a specific assumption of the particle size distribution (Bakbakhhi 2009). The kinetic parameters were estimated by fitting the model prediction to experimental data. The higher antisolvent addition rate results in promoting nucleation rate and synthesizing smaller particles. The value of kinetic parameters of ampicillin was listed in Table 9. As the results show, primary nucleation was more than secondary nucleation.

Based on the results of modeling the production of 5-FU nanoparticles through employing the GAS method in the presence of carbon dioxide (antisolvent) and DMSO (solvent) kinetically, the nucleation rate is more than the growth one. The growth rate coefficient, and growth rate order with respect to supersaturation were  $5.9007 \times 10^{-9}$  and 1.4282, respectively at an antisolvent flow rate of 2.4 mL/min. The secondary nucleation rate coefficient was  $9.6568 \times 10^{-18}$  at an antisolvent flow rate of 2.4 mL/min. In three CO<sub>2</sub> injection rates (1.6, 2, and 2.4 mL/min), the primary nucleation was higher than the secondary nucleation (Esfandiari 2014).

The kinetic modeling of phenanthrene shows the secondary nucleation rate was higher than the primary nucleation at antisolvent addition rates of 1 and 20 mL/min. This ratio is reversed when the antisolvent addition rate increases to 50 and 100 mL/min. In this modeling, the combined Lax-Wendroff/Crank Nicholson method was used (Bakbakhhi 2009). A similar trend was seen in the kinetic modeling of phenanthrene precipitation by Galerkin h-p method (Bakbakhhi et al., 2005). The results of phenanthrene experimental precipitation in Table 4 emphasize that by adding carbon dioxide, the rate of nucleation has increased and smaller particles have been produced (Bakbakhhi et al., 2005). The modeling was utilized for determining the nucleation and growth rate in the coprecipitation of naproxen with nicotinamide by using the GAS process. To this end, acetone solvent and carbon dioxide antisolvent, as well as the PR equation of state were considered (Erriguible et al., 2015). Regarding the synthesis of aspirin nanoparticles based on the GAS method, nucleation and growth rate were obtained through kinetic modeling. Following an enhancement in antisolvent flow, supersaturation power increases, and smaller particles with narrower size distribution are prepared. Furthermore, the change in solute concentration directly affects the final product particle size and its distribution (Jafari 2017).

## 2.4. Application

### 2.4.1. Nanocomposite

Some pharmaceuticals are in class II. These pharmaceuticals have high permeability and low solution in water. There are different methods to improve solubility such as size reduction, physicochemical properties modification, and drug-polymer composites production. The combination of a hydrophilic polymer and hydrophobic drug as a composite improves drug solubility (Reverchon et al., 2009, Xu et al., 2022). Polymers

commonly used in this process include polyvinylpyrrolidone, polyethylene glycol, and hydroxypropyl methylcellulose. Old methods of drug-polymer production like spray drying and solvent evaporation had problems. Some of these disadvantages are high temperatures and solvent dedication in the product. Using the GAS method can reduce these problems (Campardelli et al., 2015, Franco and De Marco 2020). One of the challenges of using supercritical fluid in micro and nanocapsules is the solubility or insolubility of pharmaceutical substances and carriers in supercritical carbon dioxide (do Nascimento Junior et al., 2021). Dittanet et al. (2016) synthesized mefenamic acid-PVP composite by implementing the GAS method at 25 and 35°C in the presence of acetone and ethanol as solvent, and carbon dioxide as antisolvent. In addition, the drug amount was considered 50 and 75 %, and the formic acid/PVP ratio was 1:1, 1:0.5, and 1:2. The results demonstrated that the solubility rate of the intended composite is 3–7-fold higher than that of mefenamic acid. Regarding the mefenamic acid/PVP ratio of 1:1, smaller particles with a narrower size distribution are detected, while larger particles are deposited when the ratio is equal to 1:0.5. A rise in polymer level in the mefenamic acid/PVP ratio (1:2) prepares a combination of small and large amorphous particles with a wide size distribution. Further, the bigger particles are precipitated by enhancing temperature. More porous particles are obtained after using the 75 % concentration of the drug compared to the 50 % one. Given that a decrease in the level leads to the superiority of the growth mechanism over the nucleation, the particles of different shapes are produced with smaller sizes (Dittanet et al., 2016). The results related to the co-precipitation of ketoconazole and 4-aminobenzoic acid through employing the GAS method in the KET to PABA ratio of 1:2, 1:1, 1:0.5 at 25–45°C in the presence of methanol, ethanol, acetone, and methanol-ethanol mixture as organic solvent reflected a promotion in the solubility rate of nanoparticles by declining temperature (Kotbantao and Charoenchaitrakool 2017). Further, paclitaxel nanoparticles were produced in the basil seed mucilage aerogel according to the GAS process, as well as the DMSO/water ratio of 4 and 6, pressure of 10–20 MPa, and carbon dioxide flow rate of 1–3 mL/min. The nanoparticle size was in the range of 82–131 nm, the mean of which diminishes by enhancing the DMSO/water ratio, and elevates by reducing pressure and carbon dioxide flow rate (Ghoreishi 2017). In another study, the drug 5-FU was loaded in hallosite nanotubes up to 43 % by using the GAS technique, which is acceptable compared to the other methods (Harikrishnan et al., 2020). Some researchers applied the GAS process to prepare hydrocortisone/polyvinyl pyrrolidone (PVP) nanocomposite. In this regard, ethanol was utilized as a solvent because of dissolving both PVP and hydrocortisone appropriately. The obtained particles possess a crystalline structure and contain 60 % PVP. Combining medicine with polymer improves properties such as solubility and dissolution rate (Corrigan and Crean 2002). The GAS method was utilized in a study to place paracetamol in Balangu seed mucilage at 0.2–0.6 M drug concentration, 40–60°C, and 8–24 MPa. The SEM, XRD, and FTIR analyses were employed to assess the product, the results of which indicated the optimum temperature, pressure, and drug level of 40°C, 8 MPa, and 0.2 M, respectively. In these optimum conditions, the drug loading is maximized up to 33 %, which reduces by increasing temperature and pressure (Falahati and Ghoreishi 2019). Nanoparticles of carbamazepine-PEG 4000 were produced by the GAS process.

Reduction of particle size and increase in solubility was the result of nanoparticles produced by this method (Moneghini et al., 2001). Pyrazinamide-PVP composite particles were coprecipitated by the GAS process. The effect of pressure, temperature, antisolvent addition rate, and polymer/drug ratio on nanocomposite characterization were studied. Increasing the pressure and temperature while decreasing the antisolvent flow rate, led to a decrease in pyrazinamide-PVP nanocomposite (Shirafkan et al., 2021).

#### 2.4.2. Co-crystal

Co-crystallization of Carbamazepine (CBZ) and Nicotinamide (NCT) and complexes of these co-crystals with  $\gamma$ -cyclodextrin (CD) with GAS were investigated. The dissolution rate of co-crystal was increased and the dissolution rate of complex co-crystal and  $\gamma$ -CD was higher than co-crystal (Shikhar et al., 2011). The GAS method was used to produce the co-crystals of itraconazole and succinic acid. The dissolution of cocrystal was 90 % in < 2 h. The co-crystal solubility generated by the gas solvent method was higher than the co-crystals by the liquid anti-solvent method (Ober and Gupta, 2012). The cocrystallization can improve the solubility of pharmaceuticals compared to the neat API. The effect of antisolvent addition rate, initial naproxen to nicotinamide molar ratio, and stirring speed on cocrystallization of naproxen and nicotinamide were studied (Neurohr et al., 2013). Box-Behnken experimental design was applied to investigate the cocrystallization of mefenamic acid and paracetamol. The effect of temperature (25–45 °C), and paracetamol to the mefenamic acid molar ratio (3:1–5:1) on dissolution rate were studied. The GAS method had higher efficiency than the slow evaporation method in this cocrystallization (Wichianphong and Charoenchaitrakool 2018). Resveratrol has many properties such as antioxidant, anticancer, antimicrobial, and cardioprotective that can be used in cancer treatment. The co-crystal of resveratrol with nicotinamide and isoniazid was produced. The dissolution rate of co-crystal was higher than pure resveratrol (Pessoa et al., 2019). Cocrystallization of itraconazole with L-malic acid by GAS was investigated at a pressure of 10.3 MPa, temperature 40 °C, and antisolvent addition rate of 1 g/min (Ober et al., 2013). In most studies, the production of co-crystal will increase its solubility compared to neat pharmaceutical.

### 3. Conclusion

In the case of the substances with low solubility in a supercritical fluid, the GAS process can be applied to prepare nano- and microparticles. Carbon dioxide can be addressed as one of the most common supercritical fluids. The factors such as temperature, pressure, antisolvent addition rate, as well as the initial concentration of the solution and the type of solvent influence the process, and particle size control and distribution. A rise in pressure and antisolvent addition flow rate leads to smaller particles, while an improvement is detected in the mean particle size at greater temperature, as well as the higher initial concentration of solute. Thermodynamic modeling is often carried out before experiments to specify temperature and pressure range in the GAS process. However, nucleation and growth rate in the process is determined through kinetic modeling. The advantage and disadvantage of supercritical fluid methods were investigated in Table 10. As previous mentioned the conventional methods have some drawbacks. However, the GAS method has become a popular approach for the generation of APIs and, more recently, pharmaceutical co-crystals as this method can remove time-consuming drying and filtration steps in addition to

generating micron- and nano-sized particles. Regarding to low capacity of GAS method, this method has good potential for special API such as inhalation pharmaceuticals. Dry powder inhaler (DPI) needs some specification like particular aerodynamic properties and tiny discrete particles that GAS method could be best choose for those goals.

### Declaration of Competing Interest

The authors declare that they have no known competing financial interests or personal relationships that could have appeared to influence the work reported in this paper.

### References

- Abuzar, S.M., Hyun, S.-M., Kim, J.-H., et al, 2018. Enhancing the solubility and bioavailability of poorly water-soluble drugs using supercritical antisolvent (SAS) process. *Int. J. Pharm.* 538, 1–13. <https://doi.org/10.1016/j.ijpharm.2017.12.041>.
- Amani, M., Ardestani, N.S., Yeganeh Majda, N., 2021. Utilization of supercritical CO<sub>2</sub> gas antisolvent (GAS) for production of Capecitabine nanoparticles as anti-cancer drug: Analysis and optimization of the process conditions. *J. CO<sub>2</sub> Util.* 46. <https://doi.org/10.1016/j.jcou.2021.101465> 101465.
- Amani, M., Saadati Ardestani, N., 2021. Investigation the phase equilibrium behavior in ternary system (CO<sub>2</sub>, DMSO, Capecitabine as anticancer drug) for precipitation of CPT Nanoparticle via the gas antisolvent supercritical process (GAS). *Brazilian J. Chem. Eng.* <https://doi.org/10.1007/s43153-021-00185-4>.
- Amaro-González, D., Mabe, G., Zabaloy, M., Brignole, E.A., 2000. Gas antisolvent crystallization of organic salts from aqueous solutions. *J. Supercrit. Fluids* 117, 249–258. [https://doi.org/10.1016/S0896-8446\(99\)00056-X](https://doi.org/10.1016/S0896-8446(99)00056-X).
- Ardestani, N.S., Amani, M., 2021. Production of Anthraquinone Violet 3RN nanoparticles via the GAS process: optimization of the process parameters using Box-Behnken design. *Dyes Pigm.* 193. <https://doi.org/10.1016/j.dyepig.2021.109471> 109471.
- Arora, D., Sedev, R., Beh, C.C., et al, 2020. Precipitation of drug particles using a gas antisolvent process on a high-pressure microfluidic platform. *Ind. Eng. Chem. Res.* 59, 11905–11913. <https://doi.org/10.1021/acs.iecr.0c01484>.
- Badens, E., Masmoudi, Y., Mouahid, A., et al, 2018. Current situation and perspectives in drug formulation by using supercritical fluid technology. *J. Supercrit. Fluids* 134, 274–283. <https://doi.org/10.1016/j.supflu.2017.12.038>.
- Bakbakhhi, Y., 2009. A discretized population balance for particle formation from gas antisolvent process: the combined Lax-Wendroff and Crank-Nicholson method. *Comput. Chem. Eng.* 33, 1132–1140. <https://doi.org/10.1016/j.compchemeng.2008.12.013>.
- Bakbakhhi, Y., Rohani, S., Charpentier, P.A., 2005. Micronization of phenanthrene using the gas antisolvent process. 1. experimental study and use of FTIR. *Ind. Eng. Chem. Res.* 44, 7337–7344. <https://doi.org/10.1021/ie050206e>.
- Bakbakhhi, Y., Rohani, S., Charpentier, P.A., 2005. Micronization of phenanthrene using the gas antisolvent process: part 2. theoretical study. *Ind. Eng. Chem. Res.* 44, 7345–7351. <https://doi.org/10.1021/ie0502077>.
- Bakbakhhi, Y., Charpentier, P.A., Rohani, S., 2006. Experimental study of the GAS process for producing microparticles of beclomethasone-17,21-dipropionate suitable for pulmonary delivery. *Int. J. Pharm.* 309, 71–80. <https://doi.org/10.1016/j.ijpharm.2005.11.008>.
- Banchero, M., 2021. Supercritical carbon dioxide as a green alternative to achieve drug complexation with cyclodextrins. *Pharmaceuticals* 14. <https://doi.org/10.3390/ph14060562>.
- Campardelli, R., Baldino, L., Reverchon, E., 2015. Supercritical fluids applications in nanomedicine. *J. Supercrit. Fluids* 101, 193–214. <https://doi.org/10.1016/j.supflu.2015.01.030>.

- Chen, K., Zhang, X., Pan, J., Zhang, W., Yin, W., 2005. Gas antisolvent precipitation of Ginkgo ginkgolides with supercritical CO<sub>2</sub>. *Powder Technol.* 152 (1), 127–132. <https://doi.org/10.1016/j.powtec.2005.01.009>.
- Cocero, M.J., Ferrero, S., 2002. Crystallization of  $\beta$ -carotene by a GAS process in batch effect of operating conditions. *J. Supercrit. Fluids* 22, 237–245. [https://doi.org/10.1016/S0896-8446\(01\)00125-5](https://doi.org/10.1016/S0896-8446(01)00125-5).
- Corrigan, O.I., Crean, A.M., 2002. Comparative physicochemical properties of hydrocortisone-PVP composites prepared using supercritical carbon dioxide by the GAS anti-solvent recrystallization process, by coprecipitation and by spray drying. *Int. J. Pharm.* 245, 75–82. [https://doi.org/10.1016/S0378-5173\(02\)00326-5](https://doi.org/10.1016/S0378-5173(02)00326-5).
- de la Fuente Badilla, J.C., Peters, C.J., de Swaan Arons, J., 2000. Volume expansion in relation to the gas-antisolvent process. *J. Supercrit. Fluids* 17, 13–23. [https://doi.org/10.1016/S0896-8446\(99\)00045-5](https://doi.org/10.1016/S0896-8446(99)00045-5).
- de Melo, S.A.B.V., Danh, L.T., Mammucari, R., et al, 2014. Dense CO<sub>2</sub> antisolvent precipitation of levothyroxine sodium: a comparative study of GAS and ARISE techniques based on morphology and particle size distributions. *J. Supercrit. Fluids* 93, 112–120. <https://doi.org/10.1016/j.supflu.2013.11.019>.
- Dittanet, P., Pothipanyakun, S., Charoenchaitrakool, M., 2016. Coprecipitation of mefenamic acid-polyvinylpyrrolidone K30 composites using gas anti-solvent. *J. Taiwan Inst. Chem. Eng.* 63, 17–24. <https://doi.org/10.1016/j.jtice.2016.03.010>.
- do Nascimento Junior, D. R., A. Taberner, E. C. d. M. Cabral Albuquerque, et al., 2021. Biopesticide Encapsulation Using Supercritical CO<sub>2</sub>: A Comprehensive Review and Potential Applications. *Molecules* (Basel, Switzerland). 26, 4003. <https://doi.org/10.3390/molecules26134003>
- Dodds, S., Wood, J.A., Charpentier, P.A., 2007. Modeling of the gas-antisolvent (GAS) process for crystallization of beclomethasone dipropionate using carbon dioxide. *Ind. Eng. Chem. Res.* 46, 8009–8017. <https://doi.org/10.1021/ie070758s>.
- Elvassore, N., Bertucco, A., Caliceti, P., 2001. Production of insulin-loaded poly(ethylene glycol)/poly(L-lactide) (PEG/PLA) nanoparticles by gas antisolvent techniques. *J. Pharm. Sci.* 90, 1628–1636. <https://doi.org/10.1002/jps.1113>.
- Erriguible, A., Neurohr, C., Revelli, A.L., et al, 2015. CocrySTALLIZATION induced by compressed CO<sub>2</sub> as antisolvent: Simulation of a batch process for the estimation of nucleation and growth parameters. *J. Supercrit. Fluids* 98, 194–203. <https://doi.org/10.1016/j.supflu.2014.12.013>.
- Esfandiari, N., 2015. Production of micro and nano particles of pharmaceutical by supercritical carbon dioxide. *J. Supercrit. Fluids* 100, 129–141. <https://doi.org/10.1016/j.supflu.2014.12.028>.
- Esfandiari, N., Ghoreishi, S.M., 2013. Kinetics modeling of ampicillin nanoparticles synthesis via supercritical gas antisolvent process. *J. Supercrit. Fluids* 81, 119–127. <https://doi.org/10.1016/j.supflu.2013.05.018>.
- Esfandiari, N., Ghoreishi, S.M., 2013. Synthesis of 5-Fluorouracil nanoparticles via supercritical gas antisolvent process. *J. Supercrit. Fluids* 84, 205–210. <https://doi.org/10.1016/j.supflu.2013.10.008>.
- Esfandiari, N., Ghoreishi, S.M., 2014. Kinetic modeling of the gas antisolvent process for synthesis of 5-fluorouracil nanoparticles. *Chem. Eng. Technol.* 37 (1), 73–80. <https://doi.org/10.1002/ceat.201300431>.
- Esfandiari, N., Ghoreishi, S.M., 2015. Ampicillin nanoparticles production via supercritical CO<sub>2</sub> gas antisolvent process. *AAPS PharmSciTech.* 16, 1263–1269. <https://doi.org/10.1208/s12249-014-0264-y>.
- Esfandiari, N., Ghoreishi, S.M., 2015. Optimal thermodynamic conditions for ternary system (CO<sub>2</sub>, DMSO, ampicillin) in supercritical CO<sub>2</sub> antisolvent process. *J. Taiwan Inst. Chem. Eng.* 50, 31–36. <https://doi.org/10.1016/j.jtice.2014.12.015>.
- Esfandiari, N., Sajadian, S.A., 2022. Experimental and modeling investigation of Glibenclamide solubility in supercritical carbon dioxide. *Fluid Phase Equilib.* 556,. <https://doi.org/10.1016/j.fluid.2022.113408> 113408.
- Falahati, M.T., Ghoreishi, S.M., 2019. Preparation of Balangu (*Lallemantia royleana*) seed mucilage aerogels loaded with paracetamol: Evaluation of drug loading via response surface methodology. *J. Supercrit. Fluids* 150, 1–10. <https://doi.org/10.1016/j.supflu.2019.04.003>.
- Foster, N., Mammucari, R., Dehghani, F., et al, 2003. Processing pharmaceutical compounds using dense gas technology. *Ind. Eng. Chem. Res.* 42, 6476.
- Franco, P., De Marco, I., 2020. The use of poly(N-vinyl pyrrolidone) in the delivery of drugs: a review. *Polymers* (Basel) 12, 1114. <https://doi.org/10.3390/polym12051114>.
- Franco, P., De Marco, I., 2021. Nanoparticles and nanocrystals by supercritical CO<sub>2</sub>-assisted techniques for pharmaceutical applications: a review. *Appl. Sci.* 11. <https://doi.org/10.3390/app11041476>.
- Fusaro, F., Mazzotti, M., Muhrer, G., 2004. Gas antisolvent recrystallization of paracetamol from acetone using compressed carbon dioxide as antisolvent. *Cryst. Growth Des.* 4, 881–889. <https://doi.org/10.1021/cg034172u>.
- Ghoreishi, S.M., Akbari, I., Hedayati, A., 2017. Preparation of basil seed mucilage aerogels loaded with paclitaxel nanoparticles by the combination of phase inversion technique and gas antisolvent process. *Nano Med. Res. J.* 2 (3), 179–188. <https://doi.org/10.22034/NMRJ.2017.03.006>.
- Giufreda, W.M., Pinto, L.F., Zanette, A.F., et al, 2014. Liquid-vapor equilibrium data of CO<sub>2</sub> + dichloromethane + medroxyprogesterone system. *Fluid Phase Equilib.* 362, 307–312. <https://doi.org/10.1016/j.fluid.2013.10.037>.
- Han, Y., Cheng, J., Ruan, N., et al, 2021. Preparation of liposomes composed of supercritical carbon dioxide-philic phospholipids using the rapid expansion of supercritical solution process. *J. Drug Delivery Sci. Technol.* 64,. <https://doi.org/10.1016/j.jddst.2021.102568> 102568.
- Harikrishnan, S., Sedev, R., Beh, C.C., et al, 2020. Loading of 5-fluorouracil onto Halloysite nanotubes for targeted drug delivery using a subcritical gas antisolvent process (GAS). *J. Supercrit. Fluids* 159,. <https://doi.org/10.1016/j.supflu.2020.104756> 104756.
- Hazaveie, S.M., Sodeifan, G., Sajadian, S.A., 2020. Measurement and thermodynamic modeling of solubility of Tamsulosin drug (anti cancer and anti-prostatic tumor activity) in supercritical carbon dioxide. *J. Supercrit. Fluids* 163,. <https://doi.org/10.1016/j.supflu.2020.104875> 104875.
- Jafari, D., Yarnezhad, I., Nowee, S.M., et al, 2015. Gas-antisolvent (GAS) crystallization of aspirin using supercritical carbon dioxide: experimental study and characterization. *Ind. Eng. Chem. Res.* 54, 3685–3696. <https://doi.org/10.1021/ie5046445>.
- Jafari, D., Nowee, S.M., Noie, S.H., 2017. A kinetic modeling of particle formation by gas antisolvent process: precipitation of aspirin. *J. Dis. Sci. Technol.* 38, 1188709. <https://doi.org/10.1080/01932691.2016.1188709>.
- Jia, J., Zhang, K., Zhou, X., et al, 2019. Berberine-loaded solid proliposomes prepared using solution enhanced dispersion by supercritical CO<sub>2</sub>: Sustained release and bioavailability enhancement. *J. Drug Delivery Sci. Technol.* 51, 356–363. <https://doi.org/10.1016/j.jddst.2019.03.021>.
- Kankala, R.K., Chen, B.-Q., Liu, C.-G., et al, 2018. Solution-enhanced dispersion by supercritical fluids: an ecofriendly nonionization approach for processing biomaterials and pharmaceutical compounds. *Int. J. Nanomed.* 13, 4227–4245. <https://doi.org/10.2147/IJN.S166124>.
- Kankala, R.K., Xu, P.-Y., Chen, B.-Q., et al, 2021. Supercritical fluid (SCF)-assisted fabrication of carrier-free drugs: an eco-friendly welcome to active pharmaceutical ingredients (APIs). *Adv. Drug Deliv. Rev.* 176,. <https://doi.org/10.1016/j.addr.2021.113846> 113846.
- Kikic, I., Lora, M., Bertucco, A., 1997. A thermodynamic analysis of three-phase equilibria in binary and ternary systems for applica-

- tions in rapid expansion of a supercritical solution (RESS), particles from gas-saturated solutions (PGSS), and supercritical antisolvent (SAS). *Ind. Eng. Chem. Res.* 36, 5507–5515. <https://doi.org/10.1021/ie970376u>.
- Knez, Ž., Pantić, M., Cör, D., et al, 2019. Are supercritical fluids solvents for the future? *Chem. Eng. Process. - Process Intensif.* 141,. <https://doi.org/10.1016/j.cep.2019.107532> 107532.
- Kotbantao, G., Charoenchaitrakool, M., 2017. Processing of ketoconazole–4-aminobenzoic acid cocrystals using dense CO<sub>2</sub> as an antisolvent. *J. CO<sub>2</sub> Util.* 17, 213–219. <https://doi.org/10.1016/j.jcou.2016.12.007>.
- Kumar, R., 2021. Numerical simulation to estimate the droplet size in aerosol solvent extraction system. *Mater. Today: Proc.* <https://doi.org/10.1016/j.matpr.2021.12.051>.
- Kumar, R., Thakur, A.K., Banerjee, N., et al, 2021. A critical review on the particle generation and other applications of rapid expansion of supercritical solution. *Int. J. Pharm.* 608,. <https://doi.org/10.1016/j.ijpharm.2021.121089> 121089.
- Kurniawansyah, F., Mammucari, R., Foster, N.R., 2017. Polymorphism of curcumin from dense gas antisolvent precipitation. *Powder Technol.* 305, 748–756. <https://doi.org/10.1016/j.powtec.2016.10.067>.
- Lee, S.Y., Abdullah, L.C., Rahman, R.A., et al, 2019. Role of polymers as crystal growth inhibitors in coprecipitation via solution-enhanced dispersion by supercritical fluids (SEDS) to improve andrographolide dissolution from standardized *Andrographis paniculata* extract. *J. Drug Delivery Sci. Technol.* 50, 145–154. <https://doi.org/10.1016/j.jddst.2019.01.026>.
- Lee, S.-Y., Jung, I.-I., Kim, J.-K., et al, 2008. Preparation of itraconazole/HP- $\beta$ -CD inclusion complexes using supercritical aerosol solvent extraction system and their dissolution characteristics. *J. Supercrit. Fluids* 44, 400–408. <https://doi.org/10.1016/j.supflu.2007.09.006>.
- Leitgeb, M., Knez, Ž., Primožič, M., 2020. Sustainable technologies for liposome preparation. *J. Supercrit. Fluids* 165,. <https://doi.org/10.1016/j.supflu.2020.104984> 104984.
- Li, K., Xu, Z., 2019. A review of current progress of supercritical fluid technologies for e-waste treatment. *J. Clean. Prod.* 227, 794–809. <https://doi.org/10.1016/j.jclepro.2019.04.104>.
- Li, Y., Yu, Y., Wang, H., et al, 2016. Effect of process parameters on the recrystallization and size control of puerarin using the supercritical fluid antisolvent process. *Asian J. Pharm. Sci.* 11, 281–291. <https://doi.org/10.1016/j.ajps.2015.12.001>.
- Liu, G., Li, J., Deng, S., 2021. Applications of supercritical antisolvent process in preparation of solid multicomponent systems. *Pharmaceutics* 13. <https://doi.org/10.3390/pharmaceutics13040475>.
- Liu, Z., Wang, J., Song, L., et al, 2002. Study on the phase behavior of cholesterol–acetone–CO<sub>2</sub> system and recrystallization of cholesterol by antisolvent CO<sub>2</sub>. *J. Supercrit. Fluids* 24, 1–6. [https://doi.org/10.1016/S0896-8446\(02\)00007-4](https://doi.org/10.1016/S0896-8446(02)00007-4).
- Long, B., Verma, V., Ryan, K.M., et al, 2021. Generation and physicochemical characterization of posaconazole cocrystals using gas antisolvent (GAS) and supercritical solvent (CSS) methods. *J. Supercrit. Fluids* 170,. <https://doi.org/10.1016/j.supflu.2020.105134> 105134.
- López-Iglesias, C., López, E.R., Fernández, J., et al, 2020. Modeling of the production of lipid microparticles using PGSS® technique. *Molecules* 25. <https://doi.org/10.3390/molecules25214927>.
- López-Iglesias, C., Quílez, C., Barros, J., et al, 2020. Lidocaine-loaded solid lipid microparticles (SLMPs) produced from gas-saturated solutions for wound applications. *Pharmaceutics* 12. <https://doi.org/10.3390/pharmaceutics12090870>.
- Lőrincz, L., Bánsághi, G., Zsemberi, M., et al, 2016. Diastereomeric salt precipitation based resolution of ibuprofen by gas antisolvent method. *J. Supercrit. Fluids* 118, 48–53. <https://doi.org/10.1016/j.supflu.2016.07.021>.
- Martausová, I., Sosna, T., Plachá, D., 2016. Modification of The Morphology of Caffeine and Cimetidine Using Supercritical CO<sub>2</sub>. [The 20th International Electronic Conference on Synthetic Organic Chemistry](https://doi.org/10.1002/9781118199999.ch10).
- Moneghini, M., Kikic, I., Voinovich, D., et al, 2001. Processing of carbamazepine–PEG 4000 solid dispersions with supercritical carbon dioxide: preparation, characterisation, and in vitro dissolution. *Int. J. Pharm.* 222, 129–138. [https://doi.org/10.1016/S0378-5173\(01\)00711-6](https://doi.org/10.1016/S0378-5173(01)00711-6).
- Muhrer, G., Lin, C., Mazzotti, M., 2002. Modeling the gas antisolvent recrystallization process. *Ind. Eng. Chem. Res.* 41, 3566–3579. <https://doi.org/10.1021/ie020070+>.
- Muller, M., Meier, U., Kessler, A., et al, 2000. Experimental study of the effect of process parameters in the recrystallization of an organic compound using compressed carbon dioxide as antisolvent. *Ind. Eng. Chem. Res.* 39, 2268.
- Muthancheri, I., Long, B., Ryan, K.M., et al, 2020. Development and validation of a two-dimensional population balance model for a supercritical CO<sub>2</sub> antisolvent batch crystallization process. *Adv. Powder Technol.* 31, 3191–3204. <https://doi.org/10.1016/j.apt.2020.06.008>.
- Najafi, M., Esfandiari, N., Honarvar, B., Arab Aboosadi, Z., 2020. Thermodynamic modeling of the gas-antisolvent (GAS) process for precipitation of finasteride. *J. Chem. Pet. Eng.* 54, 297–302. <https://doi.org/10.22059/JCHPE.2020.300747.1311>.
- Najafi, M., Esfandiari, N., Honarvar, B., Aboosadi, Z.A., 2021. Experimental investigation on finasteride microparticles formation via gas antisolvent process. *Korean Chem. Eng. Res.* 59, 455–466. <https://doi.org/10.9713/kcer.2021.59.3.455>.
- Najafi, M., Esfandiari, N., Honarvar, B., Arab Aboosadi, Z., 2021. Production of rosuvastatin calcium nanoparticles using gas antisolvent technique: experimental and optimization. *Periodica Polytech., Chem. Eng.* 65, 442–453. <https://doi.org/10.3311/PPch.16629>.
- Neurohr, C., Revelli, A.L., Billot, P., et al, 2013. Naproxen–nicotinamide cocrystals produced by CO<sub>2</sub> antisolvent. *J. Supercrit. Fluids* 83, 78–85. <https://doi.org/10.1016/j.supflu.2013.07.008>.
- Nuchuchua, O., Nejadnik, M.R., Goulooze, S.C., et al, 2017. Characterization of drug delivery particles produced by supercritical carbon dioxide technologies. *J. Supercrit. Fluids* 128, 244–262. <https://doi.org/10.1016/j.supflu.2017.06.002>.
- Ober, C.A., Gupta, R.B., 2012. Formation of Itraconazole–Succinic Acid Cocrystals by Gas Antisolvent Cocrystallization. *AAPS Pharm. Sci. Tech.* 13, 1396–1406. <https://doi.org/10.1208/s12249-012-9866-4>.
- Ober, C.A., Montgomery, S.E., Gupta, R.B., 2013. Formation of itraconazole/L-malic acid cocrystals by gas antisolvent cocrystallization. *Powder Technol.* 236, 122–131. <https://doi.org/10.1016/j.powtec.2012.04.058>.
- Padrela, L., Zeglinski, J., Ryan, K.M., 2017. Insight into the role of additives in controlling polymorphic outcome: a CO<sub>2</sub>-antisolvent crystallization process of carbamazepine. *Cryst. Growth Des.* 17, 4544–4553. <https://doi.org/10.1021/acs.cgd.7b00163>.
- Padrela, L., Rodrigues, M.A., Duarte, A., et al, 2018. Supercritical carbon dioxide-based technologies for the production of drug nanoparticles/nanocrystals – a comprehensive review. *Adv. Drug Deliv. Rev.* 131, 22–78. <https://doi.org/10.1016/j.addr.2018.07.010>.
- Pessoa, A.S., Aguiar, G.P.S., Oliveira, J.V., Bortoluzzi, A.J., Paulino, A., Lanza, M., 2019. Precipitation of resveratrol-isoniazid and resveratrol-nicotinamide cocrystals by gas antisolvent. *J. Supercrit. Fluids* 145, 93–102. <https://doi.org/10.1016/j.supflu.2018.11.014>.
- Phothipanyakun, S., Suttikornchai, S., Charoenchaitrakool, M., 2013. Dissolution rate enhancement of sulfamethoxazole using the gas anti-solvent (GAS) process. *Powder Technol.* 250, 84–90. <https://doi.org/10.1016/j.powtec.2013.10.019>.
- Rahmanzadeh Derisi, M., Esfandiari, N., 2020. Effect of solvents on the optimal thermodynamic conditions of ternary system (CO<sub>2</sub>, Alcohol, Ampicillin) in GAS process. *Iranian J. Chem. Eng.* 17 (1). <https://doi.org/10.22034/IJCHE.2020.214680.1328>.

- Revelli, A.-L., Laugier, S., Erriguible, A., et al, 2014. High-pressure solubility of naproxen, nicotinamide and their mixture in acetone with supercritical CO<sub>2</sub> as an anti-solvent. *Fluid Phase Equilib.* 373, 29–33. <https://doi.org/10.1016/j.fluid.2014.03.029>.
- Reverchon, E., Adami, R., 2006. Nanomaterials and supercritical fluids. *J. Supercrit. Fluids* 37, 1–22. <https://doi.org/10.1016/j.supflu.2005.08.003>.
- Reverchon, E., Adami, R., Cardea, S., et al, 2009. Supercritical fluids processing of polymers for pharmaceutical and medical applications. *J. Supercrit. Fluids* 47, 484–492. <https://doi.org/10.1016/j.supflu.2008.10.001>.
- Roy, C., Vrel, D., Vega-González, A., et al, 2011. Effect of CO<sub>2</sub>-antisolvent techniques on size distribution and crystal lattice of theophylline. *J. Supercrit. Fluids* 57, 267–277. <https://doi.org/10.1016/j.supflu.2011.03.002>.
- Sachett, A., Gallas-Lopes, M., Benvenuti, R., et al, 2022. Curcumin micronization by supercritical fluid: in vitro and in vivo biological relevance. *Ind. Crops Prod.* 177,. <https://doi.org/10.1016/j.indcrop.2021.114501>
- Sajadian, S.A., Ardestani, N.S., Esfandiari, N., et al, 2022. Solubility of favipiravir (as an anti-COVID-19) in supercritical carbon dioxide: an experimental analysis and thermodynamic modeling. *J. Supercrit. Fluids* 183,. <https://doi.org/10.1016/j.supflu.2022.105539>
- Sakabe, J., Uchida, H., 2022. Nanoparticle size control of theophylline using rapid expansion of supercritical solutions (RESS) technique. *Adv. Powder Technol.* 33,. <https://doi.org/10.1016/j.apt.2021.103413>
- Sakata, G.S.B., Ribas, M.M., Magro, C.D., Santos, A.E., Aguiar, G. P.S., Oliveira, J.V., Lanza, M., 2021. Encapsulation of trans-resveratrol in poly( $\epsilon$ -caprolactone) by GAS antisolvent. *J. Supercrit. Fluids* 171,. <https://doi.org/10.1016/j.supflu.2021.105164>
- Shashidhar, G.M., Pravin, G.V., Manohar, B., 2016. Nano-engineering of liposomes using a supercritical CO<sub>2</sub> mediated gas antisolvent method. *RSC Adv.* 62. <https://doi.org/10.1039/C6RA09530E>.
- Shikhar, A., Bommana, M.M., Gupta, S.S., et al, 2011. Formulation development of Carbamazepine-Nicotinamide co-crystals complexed with  $\gamma$ -cyclodextrin using supercritical fluid process. *J. Supercrit. Fluids* 55, 1070–1078. <https://doi.org/10.1016/j.supflu.2010.09.009>.
- Shirafkan, A., Nowee, S.M., Kamali, H., 2021. Gas anti-solvent coprecipitation of pyrazinamide–PVP composite particles from mixed organic solvents using supercritical CO<sub>2</sub>: Effect of process parameters. *J. Supercrit. Fluids* 178,. <https://doi.org/10.1016/j.supflu.2021.105386>
- Smirnova, I., Gurikov, P., 2017. Aerogels in chemical engineering: strategies toward tailor-made aerogels. *Annu. Rev. Chem. Biomol. Eng.* 8, 307–334. <https://doi.org/10.1146/annurev-chembioeng-060816-101458>.
- Sodeifian, G., Saadati Ardestani, N., Sajadian, S.A., et al, 2019. Experimental measurements and thermodynamic modeling of Coumarin-7 solid solubility in supercritical carbon dioxide: production of nanoparticles via RESS method. *Fluid Phase Equilib.* 483, 122–143. <https://doi.org/10.1016/j.fluid.2018.11.006>.
- Sodeifian, G., Saadati Ardestani, N., Razmimanesh, F., et al, 2020. Experimental and thermodynamic analyses of supercritical CO<sub>2</sub>-solubility of minoxidil as an antihypertensive drug. *Fluid Phase Equilib.* 522,. <https://doi.org/10.1016/j.fluid.2020.112745>
- Sodeifian, G., Alwi, R.S., Razmimanesh, F., 2022. Solubility of Pholcodine (antitussive drug) in supercritical carbon dioxide: Experimental data and thermodynamic modeling. *Fluid Phase Equilib.* 556,. <https://doi.org/10.1016/j.fluid.2022.113396>
- Sodeifian, G., Sajadian, S.A., Derakhsheshpour, R., 2022. CO<sub>2</sub> utilization as a supercritical solvent and supercritical antisolvent in production of sertraline hydrochloride nanoparticles. *J. CO<sub>2</sub> Util.* 55,. <https://doi.org/10.1016/j.jcou.2021.101799>
- Soh, S.H., Lee, L.Y., 2019. Microencapsulation and nanoencapsulation using supercritical fluid (SCF) techniques. *Pharmaceutics* 11. <https://doi.org/10.3390/pharmaceutics11010021>.
- Tandya, A., Zhuang, H.Q., Mammucari, R., et al, 2016. Supercritical fluid micronization techniques for gastroresistant insulin formulations. *J. Supercrit. Fluids* 107, 9–16. <https://doi.org/10.1016/j.supflu.2015.08.009>.
- Temelli, F., 2018. Perspectives on the use of supercritical particle formation technologies for food ingredients. *J. Supercrit. Fluids* 134, 244–251. <https://doi.org/10.1016/j.supflu.2017.11.010>.
- Tokunaga, S., Ono, K., Ito, S., et al, 2021. Microencapsulation of drug with enteric polymer Eudragit L100 for controlled release using the particles from gas saturated solutions (PGSS) process. *J. Supercrit. Fluids* 167,. <https://doi.org/10.1016/j.supflu.2020.105044>
- Türk, M., 2022. Particle synthesis by rapid expansion of supercritical solutions (RESS): current state, further perspectives and needs. *J. Aerosol Sci.* 161,. <https://doi.org/10.1016/j.jaerosci.2021.105950>
- Ulker, Z., Erkey, C., 2017. An advantageous technique to load drugs into aerogels: gas antisolvent crystallization inside the pores. *J. Supercrit. Fluids* 120, 310–319. <https://doi.org/10.1016/j.supflu.2016.05.033>.
- Wang, H.-W., Hsieh, C.-M., 2022. Prediction of solid solute solubility in supercritical carbon dioxide from PSRK EOS with only input of molecular structure. *J. Supercrit. Fluids* 180,. <https://doi.org/10.1016/j.supflu.2021.105446>.
- Warwick, B., Dehghani, F., Foster, N.R., et al, 2002. Micronization of copper indomethacin using gas antisolvent processes. *Ind. Eng. Chem. Res.* 41, 1993–2004. <https://doi.org/10.1021/ie010760y>.
- Wichianphong, N., Charoenchaitrakool, M., 2018. Application of Box-Behnken design for processing of mefenamic acid–paracetamol cocrystals using gas anti-solvent (GAS) process. *J. CO<sub>2</sub> Util.* 26, 212–220. <https://doi.org/10.1016/j.jcou.2018.05.011>.
- Xiao, Y., Wu, Z., Meng, Z., et al, 2022. Synthesis of curcumin and indocyanine green co-loaded PLLA microparticles via solution-enhanced dispersion using supercritical CO<sub>2</sub> for chemo-photothermal therapy of osteosarcoma. *J. Supercrit. Fluids* 180,. <https://doi.org/10.1016/j.supflu.2021.105462>
- Xu, Z., Lin, S., Li, Q., et al, 2022. Recent advances in techniques for enhancing the solubility of hydrophobic drugs. *Pak J Pharm Sci.* 35, 95–112.
- Yan, T., Zhang, Y., Ji, M., et al, 2019. Preparation of irbesartan composite microparticles by supercritical aerosol solvent extraction system for dissolution enhancement. *J. Supercrit. Fluids* 153,. <https://doi.org/10.1016/j.supflu.2019.104594>
- Yan, T., Tao, Y., Wang, X., et al, 2021. Preparation, characterization and evaluation of the antioxidant capacity and antitumor activity of myricetin microparticles formed by supercritical antisolvent technology. *J. Supercrit. Fluids* 175,. <https://doi.org/10.1016/j.supflu.2021.105290>
- Yeo, S.D., Lim, G.B., Debenedetti, P.G., et al, 1993. Formation of microparticulate protein powders using a supercritical fluid antisolvent. *Biotechnol. Bioeng.* 41, 346.